© 2016. Published by The Company of Biologists Ltd | Development (2016) 143, 4521-4532 doi:10.1242/dev.141291

RESEARCH ARTICLE

Sensory evolution in blind cavefish is driven by early embryonic events during gastrulation and neurulation

Hélène Hinaux, Lucie Devos, Maryline Blin, Yannick Elipot, Jonathan Bibliowicz, Alexandre Alié and Sylvie Rétaux*

ABSTRACT

Natural variations in sensory systems constitute adaptive responses to the environment. Here, we compared sensory placode development in the blind cave-adapted morph and the eyed river-dwelling morph of *Astyanax mexicanus*. Focusing on the lens and olfactory placodes, we found a trade-off between these two sensory components in the two morphs: from neural plate stage onwards, cavefish have larger olfactory placodes and smaller lens placodes. In a search for developmental mechanisms underlying cavefish sensory evolution, we analyzed the roles of Shh, Fgf8 and Bmp4 signaling, which are known to be fundamental in patterning the vertebrate head and are subtly modulated in space and time during cavefish embryogenesis. Modulating these signaling systems at the end of gastrulation shifted the balance toward a larger olfactory derivative. Olfactory tests to assess potential behavioral outcomes of such developmental evolution revealed that *Astyanax* cavefish are able to respond to a 10^5-fold lower concentration of amino acids than their surface-dwelling counterparts. We suggest that similar evolutionary developmental mechanisms may be used throughout vertebrates to drive adaptive sensory specializations according to lifestyle and habitat.

KEY WORDS: Lens placode, Olfactory placode, Trade-off, Complex trait, Signaling, Olfactory skills

INTRODUCTION

Animals rely on their sensory systems to perceive relevant stimuli in their environment. Natural selection favors sensory systems that are adapted to stimuli used for survival and reproduction. In line with this idea, there are numerous examples in the literature of sensory specialization in animals according to their habitat. This concerns both external sensory organs and brain areas that process the sensory information. However, not much is known about how existing sensory systems evolve, particularly in terms of size, to fit a specific environment.

To cite a few examples, diurnal rodents have a larger proportion of cerebral cortex devoted to visual areas than nocturnal rodents, the latter having a larger part of their cortex devoted to somatosensory and auditory areas (Campi and Krubitzer, 2010; Krubitzer et al., 2011). Among cichlid fish in African lakes, the relative size of brain regions in different species varies according to the environment and feeding habits (Pollen et al., 2007). Sensory organs also vary greatly among species. Classical cases include the small eyes but highly developed olfactory epithelium of sharks (Collin, 2012), the vibrissae-like tactile hair covering the otherwise hairless skin of the underground-living naked mole rat (Crish et al., 2003; Park et al., 2003; Sarko et al., 2011) or the variation in the number of lateral line neuromasts in sticklebacks depending on their stream versus marine, or benthic versus limnetic, habitat (Wark and Peichel, 2010).

Of note, the evolution of a particular sensory organ is often discussed with no consideration of the role played by other senses, but recent analyses have revealed co-operations and trade-offs among senses (Nummela et al., 2013). Developmentally, this implies that the control of the size of sensory organs is tightly regulated during embryogenesis and later, and that this regulation is somehow coordinated between the different organs.

In cave animals from all phyla, a striking blind (and de-pigmented) phenotype is repeatedly observed. In the blind cavefish (CF) of the species *Astyanax mexicanus*, which can be advantageously used in developmental comparative analyses because sighted surface fish (SF) of the same species are available (Jeffery, 2008, 2009), the eyes are regressed in adults, but sensory compensations have been reported: CF have more taste buds (chemosensory) (Schemmel, 1967; Varatharasan et al., 2009; Yamamoto et al., 2009) and more head neuromasts (mechanosensory) (Jeffery et al., 2000; Yoshizawa and Jeffery, 2011) than SF. Also consistent with this idea, CF are better at finding food in the dark (Espinasa et al., 2014; Hüppop, 1987) and seem more sensitive to food-related cues than SF (Bibliowicz et al., 2013; Protas et al., 2008). Although the olfactory system (chemosensory) was initially thought to be anatomically and physiologically unchanged in CF (Riedel and Krug, 1997; Schemmel, 1967), later studies found that naris opening is larger in troglomorphic animals (Bibliowicz et al., 2013; Yamamoto et al., 2003), suggesting a possible link between increased food finding capabilities and olfactory specialization. From an evolutionary perspective, these changes in different sensory modules could be either uncoupled or be the result of common selection pressures, acting at developmental and genetic levels (Franz-Odendaal and Hall, 2006; Wilkens, 2010).

Importantly, in *Astyanax* CF the eyes first develop almost normally during embryogenesis before they then degenerate. The triggering event for eye degeneration is lens apoptosis (Alunni et al., 2007; Yamamoto and Jeffery, 2000). The lack of expression of αA-crystallin, a lens differentiation gene (Behrens et al., 1998; Strickler et al., 2007), probably contributes to the apoptotic phenotype in CF (Hinaux et al., 2014; Ma et al., 2014). However, CF eyes are also smaller than SF eyes from embryonic stages onward (Hinaux et al., 2011; Strickler et al., 2001). What are the developmental mechanisms underlying the regulation of sensory organ size in CF? Previous work has shown that increased Shh signaling and heterochronic Fgf8 signaling in CF have pleiotropic effects on neural development: Shh is indirectly responsible for lens apoptosis (Yamamoto et al., 2004) and also impacts the number of taste buds

DECA group, Paris-Saclay Institute of Neuroscience, CNRS, Université Paris Sud, Université Paris-Saclay, Avenue de la terrasse, Gif-sur-Yvette 91198, France.

*Author for correspondence (retaux@inaf.cnrs-gif.fr)

Received 20 June 2016; Accepted 20 October 2016

Development (2016) 143, 4521-4532 doi:10.1242/dev.141291

(Yamamoto et al., 2009), while Shh and Fgf8 influence the relative sizes of the domains of the neural plate and neural tube that are fated to contribute to the retina or to other brain parts (Menuet et al., 2007; Pottin et al., 2011).

Shh and Fgf signaling are also known to affect the development of the placodal region in other vertebrate model species (Bailey et al., 2006; Dutta et al., 2005). The placodes correspond to a region surrounding the neural plate that generates the sensory organs of the head in vertebrates, including the lens, the olfactory epithelium, the otic vesicle and the lateral line (Schlosser, 2006; Streit, 2007, 2008; Torres-Paz and Whitlock, 2014; Whitlock and Westerfield, 2000). Here, we investigated the development of the *Astyanax* CF placodal region, with a particular focus on the lens and olfactory placodes. We report significant differences in patterning between CF and SF embryos and show that Shh, Fgf and Bmp4 modifications contribute to opposite changes in the size of the lens and olfactory placodes in CF. Further comparing olfactory behavior of the two morphs, we uncover outstanding olfactory skills in CF, confirming their functional olfactory specialization.

RESULTS

Early patterning of the placodes

We compared placodal field patterning in Pachón CF and SF embryos at the end of gastrulation/beginning of neurulation (Fig. 1). At 10 hours post fertilization (hpf), the shape and size of the neural plate border domain labeled by *Dlx3b* was similar in SF and CF (Fig. 1A,A′). Inside this *Dlx3b*-positive border, the anterior neural plate markers *Zic1* and *Pax6*, which label the 'eye field' and presumptive forebrain, are prominently expressed (Fig. 1B-C′). At the placodal level, the anteriormost part of the *Pax6*-positive presumptive lens placode territory was lacking in CF embryos, resulting in a smaller lens territory (Fig. 1C-C″). The width (mediolateral extension) of the *Pax6* lens placode domain was similar in SF and CF, consisting of 2-3 cell diameters (Fig. 1C-D′). Examination of the anteriormost placodal region using the *Dlx3b* marker on frontal views also revealed robust differences, with its domain being anteriorly expanded in CF embryos (Fig. 1E-E″, and see below). Thus, early anterior placodal patterning is modified in CF embryos, and the lens placode is reduced in size.

Slightly later, at 12 hpf (end of neurulation) and 16 hpf (mid-somitogenesis), *Dlx3b* expression was progressively reduced to the presumptive olfactory and otic placode and to the adhesive organ or casquette (Fig. 2A-B′, Fig. S1A) (Pottin et al., 2010). The *Dlx3b*-negative ventrolateral head region corresponding to the forming eye vesicle was reduced in CF (Fig. 2A-A″), whereas the *Dlx3b*-positive dorsolateral domain corresponding to the olfactory placode was much larger in CF (Fig. 2B-B″). This was confirmed by the olfactory marker *Eya2* (Fig. 2C-C″).

From 20 hpf onwards, the lens mass was clearly identified using *Pitx3* (Fig. 2D,D′), which is expressed throughout the lens in both SF and CF (Fig. 2F,G), therefore providing a good proxy for lens size. The *Pitx3*-positive lens area was much smaller in CF than in SF embryos (Fig. 2D″).

In parallel, the size of the olfactory epithelium (OE) derived from the olfactory placode was assessed after hatching by Olfactory marker protein (*OMP*) expression (Fig. 2E,E′). The area where

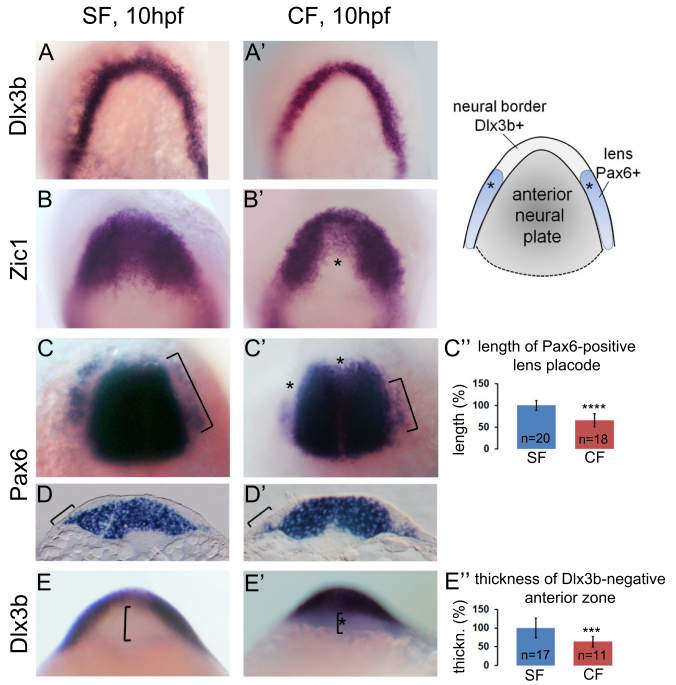

Fig. 1. Early patterning of the anterior placodes and neural plate at 10 hpf. (A-E′) SF (left) and CF (right) embryos after *in situ* hybridization for the indicated genes. (A-C′) Dorsal views, anterior to the top; (D,D′) transverse sections; (E,E′) frontal views. Brackets indicate regions of interest. Asterisks indicate differences between SF and CF. The scheme on the right helps the interpretation of gene expression patterns. (C″,E″) Quantification of gene expression domains in SF and CF for 10 hpf embryos. In this and following figures, numbers in bars indicate the number of embryos used for quantification, and data are mean±s.e.m. ****P<0.0001, ***P<0.001, Mann–Whitney test.

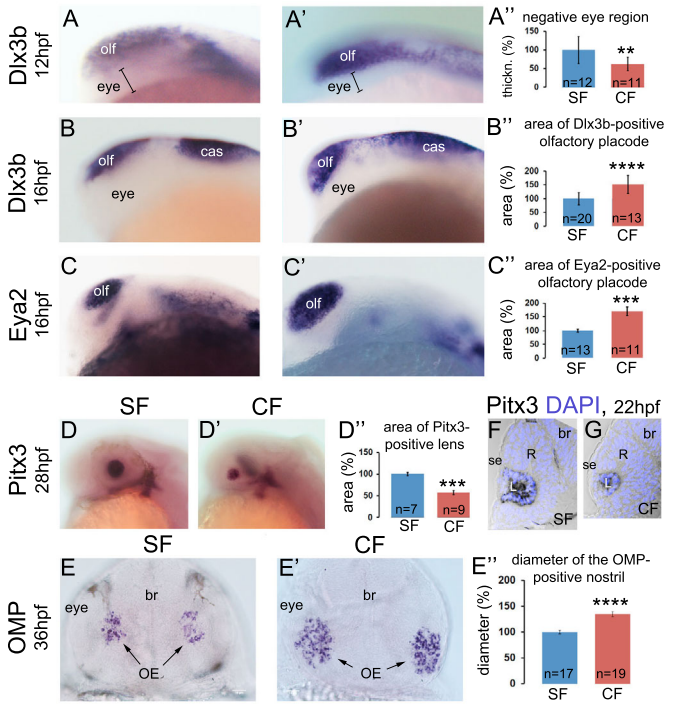

Fig. 2. Late patterning of the anterior placodes. (A-E′) SF (left) and CF (right) embryos showing expression of the indicated genes at the indicated stages. (A-D′) Lateral views, anterior to the left; (E,E′) frontal views. (F,G) Transverse sections through the eyes, with DAPI (blue) nuclear counterstaining. (A″-E″) Quantification of gene expression domains in SF and CF. Measurements were made on lateral (A″-D″) or frontal (E″) views. **P<0.01, ***P<0.001, ****P<0.0001, Mann–Whitney test. br, brain; cas, casquette; L, lens; OE, olfactory epithelium; olf, olfactory placode; R, retina; se, surface ectoderm.

Development (2016) 143, 4521-4532 doi:10.1242/dev.141291

OMP-positive neurons are scattered in a salt and pepper pattern was much larger in CF than in SF (Fig. 2E″), and this difference was maintained at 64 hpf (Fig. S2A).

We also examined the anteriormost derivatives of the placodal field, fated to become the adenohypophysis/pituitary in vertebrates (Dutta et al., 2005). Unfortunately, none of the three *Astyanax* Pitx genes that we cloned was expressed in the pituitary (Fig. S3A-C). We therefore isolated *Lhx3*, a LIM-homeodomain transcription factor considered as an early and specific pituitary marker. *Lhx3* expression starts at ∼24 hpf in *Astyanax* (not shown). At 28 hpf, the size of the *Lhx3*-positive domain and the number of *Lhx3*-positive cells were similar in SF and CF (Fig. S1B), suggesting that, anteriorly, only the olfactory and the lens derivatives vary in size between the two morphs. Finally, the posterior otic placode was identical in size in CF and SF according to *Dlx3b* expression (Fig. S1A), suggesting that only the anterior placodes are modified in CF.

Altogether, these patterning data suggest that the olfactory placode and epithelium are continuously enlarged in CF at the expense of a reduction of the lens placode and mass.

A genetic link between lens and olfactory derivative size control in CF?

To test directly a genetic link between the opposite variations in olfactory and lens sizes in CF, we established crosses to generate first (F1) and second (F2) generation hybrids. In 36 hpf F1 hybrids resulting from SF×Pachón CF crosses, the size of the lens (Fig. 3A,A′) and the size of the OE (Fig. 3B,B′) were intermediate between those of a SF and a CF larva of the same age. In 36 hpf F2 hybrids resulting from crosses between two F1 parents, the lens and OE volume were measured concomitantly in single individuals (n=33) on confocal images (Fig. 3C). There was no correlation between lens size and OE size (Fig. 3C′). This suggests that the control of OE size and lens size are complex traits, with a multigenic determinism. These results are in line with previous findings that at least six QTL are involved in the control of lens size (Protas et al., 2007).

Signaling systems and the control of placodal patterning and fate in CF

We next investigated the origins of the modifications of placodal patterning in CF. That differences were observed as early as 10 hpf suggested that they resulted from modifications during gastrulation. Shh hyper-signaling from the notochord and *Fgf8* heterochronic (earlier) expression in the anterior neural ridge are known in CF (Pottin et al., 2011; Yamamoto et al., 2004). In addition, the differences that we observed in the anterior placode region (Fig. 1E,E′) suggested that signaling from the prechordal plate (pcp), an endomesodermal structure with important signaling properties for induction and patterning of the forebrain (Kiecker and Niehrs, 2001), might be affected in CF.

At the end of gastrulation (9.5-10 hpf), the pcp abuts the anterior limit of the embryonic axis, being just rostral to the *Shh*-expressing notochord and just ventral to the *Dlx3b*- and *Fgf8*-expressing anterior neural border (Fig. 4A,B). *Bmp4* expression in the *Astyanax* pcp can be subdivided into the polster (anterior, round in shape, *Shh*-negative) and posterior prechordal plate (ppcp, elongated in shape, *Shh*-positive) domains. *Bmp4* spatiotemporal expression was compared in the two morphs between 9.5 hpf and 11 hpf (Fig. 4A). In SF, *Bmp4* was expressed either in polster only (the majority of embryos) or in polster and ppcp (Fig. 4A-C, Fig. S4A). Conversely, in CF, a majority of embryos showed expression in the ppcp only, and confocal examination confirmed the absence of *Bmp4* expression in the polster for many of them (Fig. 4B). Importantly, the polster, as a structure, is present in CF and the migration of the pcp appears similar in the two morphs as (1) a few CF embryos did show some *Bmp4* staining in the polster (Fig. 4C, Fig. S4A) and (2) the expression of other genes, such as *Pitx1* (Fig. S4C) or the recognized pcp marker *goosecoid* (*Gsc*), was present in SF and CF

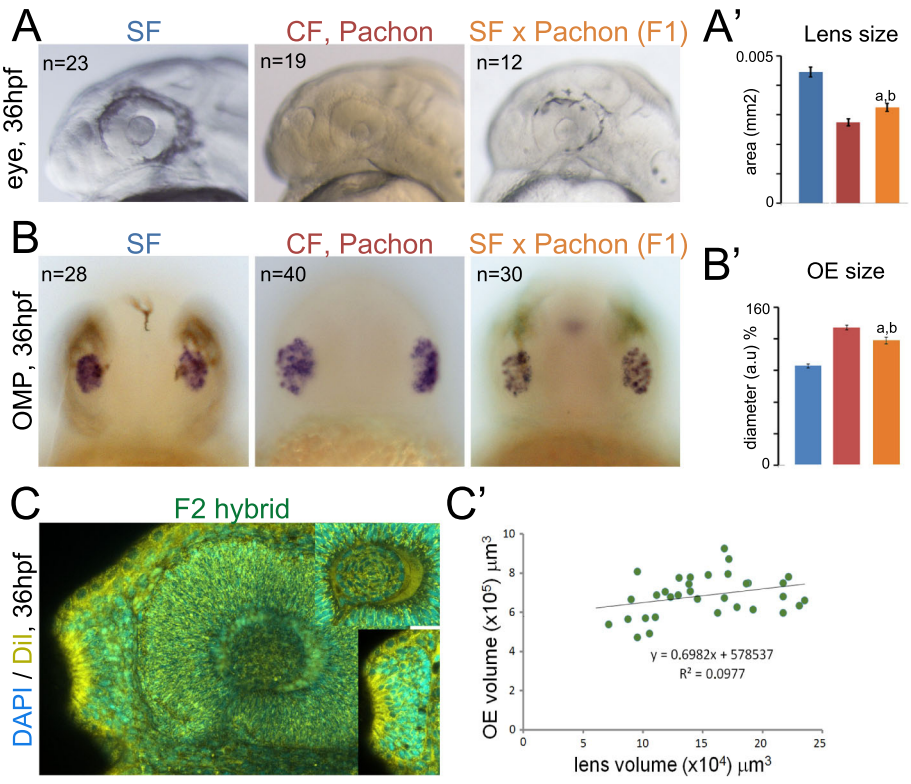

Fig. 3. Lens and OE size in F1 and F2 hybrids. (A,B) Images of the head (A) or after *in situ* hybridization for *OMP* in frontal views (B) of 36 hpf SF, CF and F1 hybrids. (A′) Lens measurements in 36 hpf larvae. a, different from SF (P<0.0001); b, different from CF (P=0.0056). SF and CF lens sizes are also significantly different (P<0.0001). Mann–Whitney tests. SF, blue; CF, red; F1 hybrid, orange. (B′) OE size in the three types of larvae. a, different from SF (P<0.0001); b, different from CF (P=0.0046). SF and CF OEs are also significantly different (P<0.0001). Mann–Whitney tests. (C) Confocal stack and image (inset) of 36 hpf F2 hybrids after DAPI/DiI staining, showing the lens and OE of a single embryo, on which OE and lens volumes were measured. (C′) Correlation plot between OE and lens volume.

Development (2016) 143, 4521-4532 doi:10.1242/dev.141291

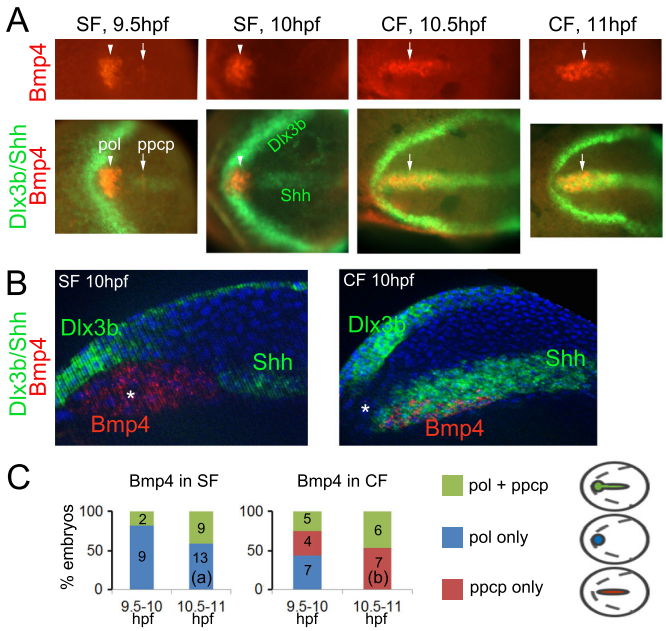

Fig. 4. *Bmp4* expression dynamics in prechordal plate. (A) Expression of *Bmp4* between 9.5 hpf and 11 hpf in SF and CF embryos after triple *in situ* hybridization for *Bmp4* (red), *Dlx3b* (green) and *Shh* (green). Anterior is to the left. (Top) Dorsal views of *Bmp4* expression in the polster (pol, arrowhead) and posterior prechordal plate (ppcp, arrow). (Bottom) Merged images of the entire neural plate. *Dlx3b* labels the neural plate border, and *Shh* is expressed at the ventral midline (ppcp and notochord). (B) Confocal sections through the sagittal plane of 10 hpf SF (left) and CF (right) embryos after triple *in situ* hybridization for *Bmp4* (red), *Dlx3b* (green) and *Shh* (green), showing exclusive or overlapping expression domains between the three genes. Anterior is to the left. Asterisk, polster. (C) Distribution of *Bmp4* pattern types in SF and CF between 9.5 hpf and 11.5 hpf. Color codes match the patterns schematized on the right and numbers in bars give the numbers of embryos examined. The distribution is significantly different between SF and CF at 10.5-11 hpf. a, P=0.0006 for expression in polster only in SF versus CF; b, P=0.00026 for expression in ppcp only in SF versus CF; Fisher's exact test.

with comparable dynamics (Fig. S5). Thus, significant differences in the dynamics of *Bmp4* expression inside the pcp exist between CF and SF (see Fig. 4C legend).

Present and previous results prompted us to investigate whether the multiple changes observed in Shh, Fgf8 and Bmp4 signaling systems are responsible for sensory placode and organ size variations in CF. We designed strategies to assess the influences of Shh and Fgf8, which correspond to quantitative differences in space and time between SF and CF, or the influence of Bmp4, which relates to qualitative differences in expression dynamics inside the pcp between the two morphs.

To test the influence of *Shh* heterotopy and *Fgf8* heterochrony, CF embryos were treated with cyclopamine [an antagonist of the Shh receptor Smoothened (Chen et al., 2002)] or with SU5402 [an antagonist of Fgf receptor signaling (Mohammadi et al., 1997)], respectively, between 6 hpf (shield) and 10 hpf (end of gastrulation), and the sizes of their lens and olfactory placodes were measured at later stages. Cyclopamine (100 µM) resulted in a 19% increase in lens size, as measured at 28 hpf using *Pitx3* as marker (Fig. 5A-A‴). Although significant, the cyclopamine-induced increase in lens size resulted in a lens that was still smaller than in SF. Inhibition of Fgf signaling with 0.5 µM SU5402 had no significant effect on lens size (Fig. 5A‴). By contrast, cyclopamine and SU5402 both induced a significant reduction in the size of the olfactory placode (−25% and −21%, respectively), as measured at 16 hpf using the *Eya2* marker (Fig. 5B-B‴). Notably, the reduction after both treatments in CF resulted in an olfactory placode of identical size to that of SF embryos.

Because the *Bmp4* differences in CF and SF relate to subtle expression dynamics and to the position of the signal within the pcp, their impact was not testable through pharmacological manipulation during a specific time window. An alternative experimental design was used: Bmp4 protein injections were performed at 10 hpf, aiming at anteriorizing or posteriorizing Bmp4 signaling in CF and SF embryos, and thereby mimicking one morph's situation in the other (Fig. 5C). Anterior injections of Bmp4 in CF produced an increase in lens size (+15%; Fig. 5D-D″,F) and a reduction in olfactory placode size (−16%; Fig. 5E-E″,F), suggesting opposite effects of polster Bmp4 signaling on the two sensory derivatives. The CF olfactory placode was also reduced after posterior Bmp4 injection (−16%, Fig. 5E″), suggesting that olfactory derivatives are negatively affected by high levels of Bmp4 signaling at the neural plate stage. Moreover, unlike injections in CF, anterior or posterior injection of Bmp4 in SF did not change lens or olfactory sizes (Fig. 5D″,E″), pointing to the specific lack of Bmp4 in the anterior polster part of the pcp as partly responsible for the small size of the lens in CF, or to the possibility that lens size might already be maximal in SF and therefore cannot be further increased, and that olfactory size might be minimal and cannot be further decreased.

Continued olfactory specialization in juvenile CF

Because an enlargement of the OE in CF may be of functional importance for survival in the dark, we examined whether it remained larger than in SF at juvenile stages. We used the $G_{\alpha olf}$ olfactory marker on 1-month-old larvae, when the OE is not yet folded inside the naris (Hansen et al., 2004; Wekesa and Anholt, 1999) (Fig. 6A,B,D,E). The size of the $G_{\alpha olf}$-positive OE and of the naris opening were significantly larger in CF than in SF (Fig. 6G) (OE, 1.36-fold; naris opening, 1.31-fold; values corrected to body length). Cell counts on sections showed an increased number of cells in the CF OE (Fig. 6H). Labeling of the olfactory projection by insertion of a crystal of lipophilic DiI in the olfactory cup revealed a conserved organization of the olfactory projection onto olfactory bulb glomeruli (Fig. 6C,F). The shape of the OE was consistently round in SF and oval in CF (compare Fig. 6A-F). The olfactory nerve was also longer in CF, which is probably due to the difference in size and shape of the jaw and skull (see also Fig. 7F).

Establishing a sensitive olfactory test

To compare the olfactory skills of 1-month-old juvenile CF and SF (5-6 mm in length), we designed an olfaction assay using amino acids as odorant molecules, in the dark with infrared recordings (Fig. 7A,B, Fig. S6A-C, Movie 1, and see the Materials and Methods). Amino acids are potent feeding cues in teleosts (Byrd and Caprio, 1982; Friedrich and Korsching, 1997) and have been used to test olfactory sensitivity and discrimination (Koide et al., 2009; Lindsay and Vogt, 2004; Vitebsky et al., 2005).

Depending on the fish species and the amino acid, millimolar to nanomolar concentrations trigger neuronal activation in the olfactory system (Dolensek and Valentincic, 2010; Evans and Hara, 1985; Friedrich and Korsching, 1997; Korsching et al., 1997; Vitebsky et al., 2005). We used these concentrations as a starting point. Perfusion of a 10^{-3} M to 10^{-5} M stock of alanine or serine resulted in a strong attractive response (positive preference index score) in both morphs (Fig. 7C,D).

Interestingly, when the test was performed in the light and the quantification of the response was carried out for longer, we

Development (2016) 143, 4521-4532 doi:10.1242/dev.141291

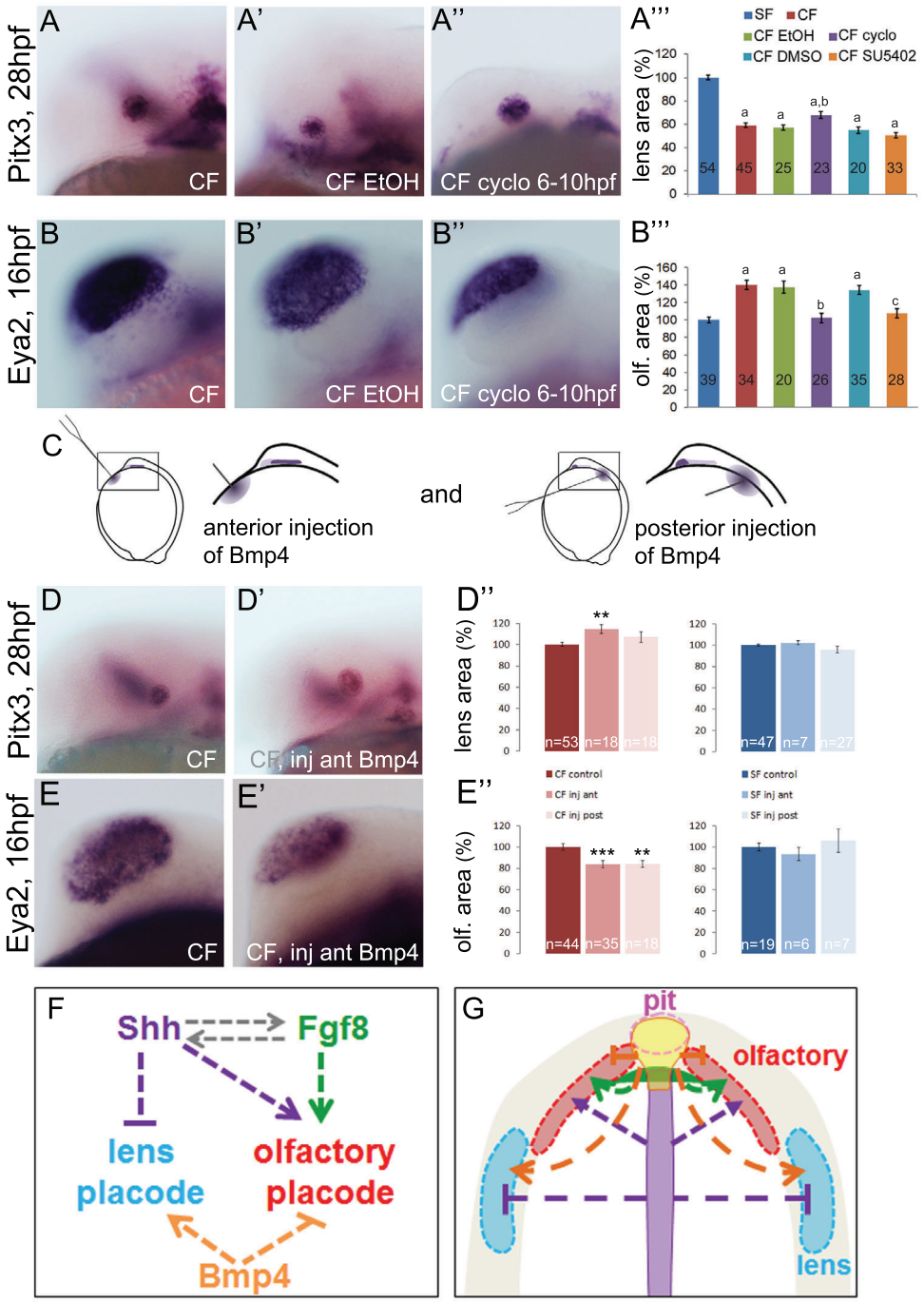

Fig. 5. Impact of early signaling systems on lens and olfactory size. (A-B″) Images of 28 hpf CF embryos showing the *Pitx3*-expressing lens and of 16 hpf CF embryos showing the *Eya2*-expressing olfactory placode, after the indicated treatments. Lateral views, anterior to the left. (A‴) Quantification of lens size according to *Pitx3* expression. Cyclo, 100 µM cyclopamine; SU5402, 0.5 µM SU5402 treatment between 6 hpf and 10 hpf. Ethanol and DMSO (vehicles) had no effect on lens size. Although relatively severely affected for head development (A″), embryos treated with cyclopamine show larger lenses. a, different from SF (P<0.0001); b, different from CF treated with ethanol (P<0.01) and from CF (P<0.05). Mann–Whitney tests. (B‴) Quantification of olfactory placode size according to *Eya2* expression. Ethanol and DMSO had no effect on olfactory placode size. a, different from SF (P<0.0001); b, different from CF treated with ethanol (P<0.001) and from CF (P<0.0001) and not different from SF; c, different from CF treated with DMSO (P<0.001) and from CF (P<0.0001) and not different from SF. Mann–Whitney tests. (C) Experimental design for Bmp4 protein injections at 10 hpf. (Left) Orientations and paths for injecting needles to target the anteriormost region of the head or the more posterior ventral midline. (Right) Magnification of the head region, where the endogenous morph-specific expression pattern of *Bmp4* in the pcp is also depicted by the intensity of purple. (D-E′) Images of 28 hpf CF embryos showing the *Pitx3*-expressing lens and of 16 hpf CF embryos showing the *Eya2*-expressing OE in the indicated conditions. (D″) Quantification of lens size after Bmp4 injections. **P<0.01, Mann–Whitney test. (E″) Quantification of olfactory placode size after Bmp4 injections. **P<0.01, ***P<0.001, Mann–Whitney test. (F) Proposed regulatory network depicting Shh, Fgf8 and Bmp4 signaling effects on lens versus olfactory placode specification and fate. The previously described cross-talk between Shh and Fgf is also indicated (gray; from Pottin et al., 2011).The dotted arrows indicate that effects could be indirect. (G) Signaling network transposed into the embryonic context. In CF embryos, Fgf8 heterochrony and Shh hyper-signaling promote enlargement of the olfactory placode and reduction of the lens placode territory, and the lack of anterior Bmp4 signaling by the polster also contributes to the reduction of the lens domain and the increase of the olfactory domain.

Development (2016) 143, 4521-4532 doi:10.1242/dev.141291

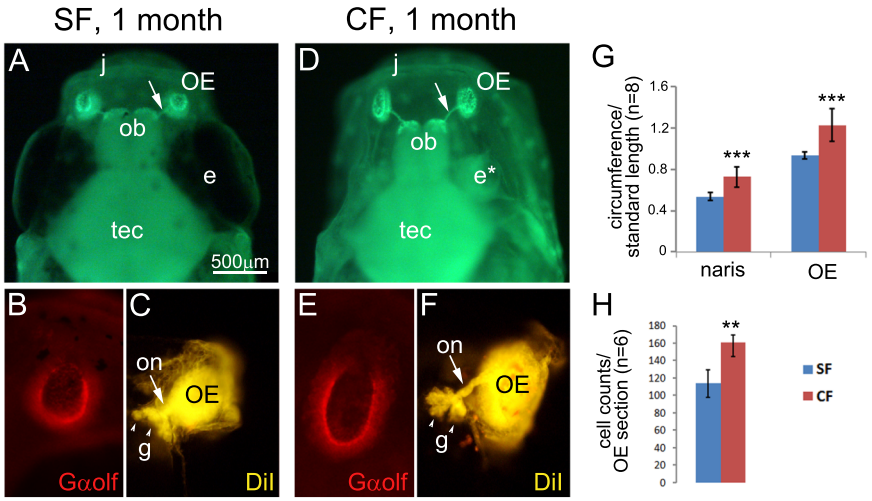

Fig. 6. Organization and size of the olfactory apparatus in juveniles. (A-F) Anatomy of the olfactory apparatus. OE sensory neurons project onto the olfactory bulbs (ob) through the olfactory nerve (on, arrow). (A,B,D,E) $G_{\alpha olf}$ immunofluorescence (green or red) on 1-month-old SF and CF. (A,D) Dorsal views (anterior is up) of the heads; (B,E) high magnification at OE level. (C,F) The olfactory sensory projection after insertion of a crystal of DiI in the olfactory cup of 2-week-old larvae, visualizing olfactory bulb glomeruli (g, arrowheads). Note the differences in OE size and shape (larger and oval in CF) and optic nerve length (longer and thicker in CF). j, jaw; e, eye (asterisk indicates degenerated eye in CF); tec, optic tectum. (G,H) Quantification of OE size (G) and counting of OE cells (H) in 1-month-old SF and CF. Measurements were performed on juveniles of equivalent size and normalized to standard length (G). $G_{\alpha olf}$ was used to measure OE/naris opening circumferences and DAPI-stained sections were used for cell counts. ***P<0.0001, **P<0.01, Mann–Whitney test.

observed that, in contrast to CF, SF were only transiently attracted to the odorant compartment for ∼4 min, and then swam randomly in the box (Fig. 7E). We interpret this observation as vision interfering with olfactory-driven behavior: SF can see that no food is present despite the food-related odor, and do not persist in their behavioral response. This confirms the importance of the visual sensory modality in controlling SF behavior, and the accuracy of the behavioral set-up.

Attraction to amino acids is mediated by the OE

In both bony and cartilaginous fish, olfaction is used to localize food sources, breeding partners and predators, as well as for communication and learning, while gustation is primarily involved in feeding, including oral processing and evaluating food palatability through direct contact (Collin, 2012; Derby and Sorensen, 2008). Chemosensory detection of amino acids depends on both gustatory and olfactory sensory modalities (Hara, 1994). In most fish species, the detection threshold of the taste buds is in the micromolar range (Hara, 1994, 2006, 2015), higher than the concentrations used here. However, as CF possess more taste buds than SF on their lips and face (Schemmel, 1967; Varatharasan et al., 2009; Yamamoto et al., 2009), we needed to ascertain that the observed response to amino acids was truly olfactory mediated. We chemically ablated the surface of the OE by application of a Triton X-100 solution onto the naris (Iqbal and Byrd-Jacobs, 2010), which resulted in the disappearance of $G_{\alpha olf}$ immunoreactivity (Fig. 7F). Olfactory responses were measured on bilaterally OE-ablated fish using 10^{-5} M alanine, which induces a strong attraction in both morphs in normal fish (see Fig. 7C). OE-ablated SF and CF did not respond to the odor at any time point (Fig. 7G). Importantly, this lack of attraction was not due to a lack of exploratory behavior (Fig. S6D). Thus, at the concentrations used, the behavioral assay measures olfactory-mediated, but not gustatory-mediated, responses.

CF have a more sensitive olfactory response

To determine and compare the threshold concentrations of amino acid detection of the two morphs, we repeated the experiments at progressively decreasing concentrations. Alanine or serine at 10^{-6} M still resulted in a robust attraction of CF to the amino acid source, whereas SF no longer displayed such attraction (Fig. 8A,B). The result was identical for the two amino acids, and the lack of response in SF was not due to a difference in swimming exploratory behavior (Fig. S7). As expected, SF did not respond to even lower concentrations (10^{-7} M alanine, not shown). To determine the CF discrimination threshold, we further decreased the alanine concentration to 10^{-7} M (not shown), 10^{-9} M, 10^{-10} M and 10^{-11} M. Remarkably, the CF detection threshold was 10^{-10} M (Fig. 7C). Thus, CF are able to respond to 10^{5}-fold lower concentrations of amino acids than SF.

DISCUSSION

Using *Astyanax* CF as 'natural mutants' we uncovered early developmental origins of natural variations in sensory systems. We discuss our findings in terms of a specific understanding of the developmental mechanisms underlying the CF phenotype, and in terms of a more general understanding of sensory development and evolution in vertebrates.

Specific considerations of CF developmental evolution and phenotype

Adult cavefish are blind. During embryonic and larval development, the two main components of their eyes are affected: the retina is small and lacks a ventral quadrant (Pottin et al., 2011) and the lens undergoes apoptosis, which triggers degeneration of the entire eye (Yamamoto and Jeffery, 2000). Moreover, the CF lens enters apoptosis even if transplanted into an SF optic cup (Yamamoto and Jeffery, 2000), suggesting that CF lens defects could stem from early embryonic events. Here, we show that from the earliest possible stage of lens tracing, using transient expression of *Pax6* at the pan-placodal stage when placodal precursors are still plastic to give rise to several sensory derivatives (Bailey and Streit, 2006; Dutta et al., 2005; Martin and Groves, 2006; Sjödal et al., 2007), the presumptive territory (and hence the number of precursors) of the lens is reduced in CF as compared with SF embryos.

Development (2016) 143, 4521-4532 doi:10.1242/dev.141291

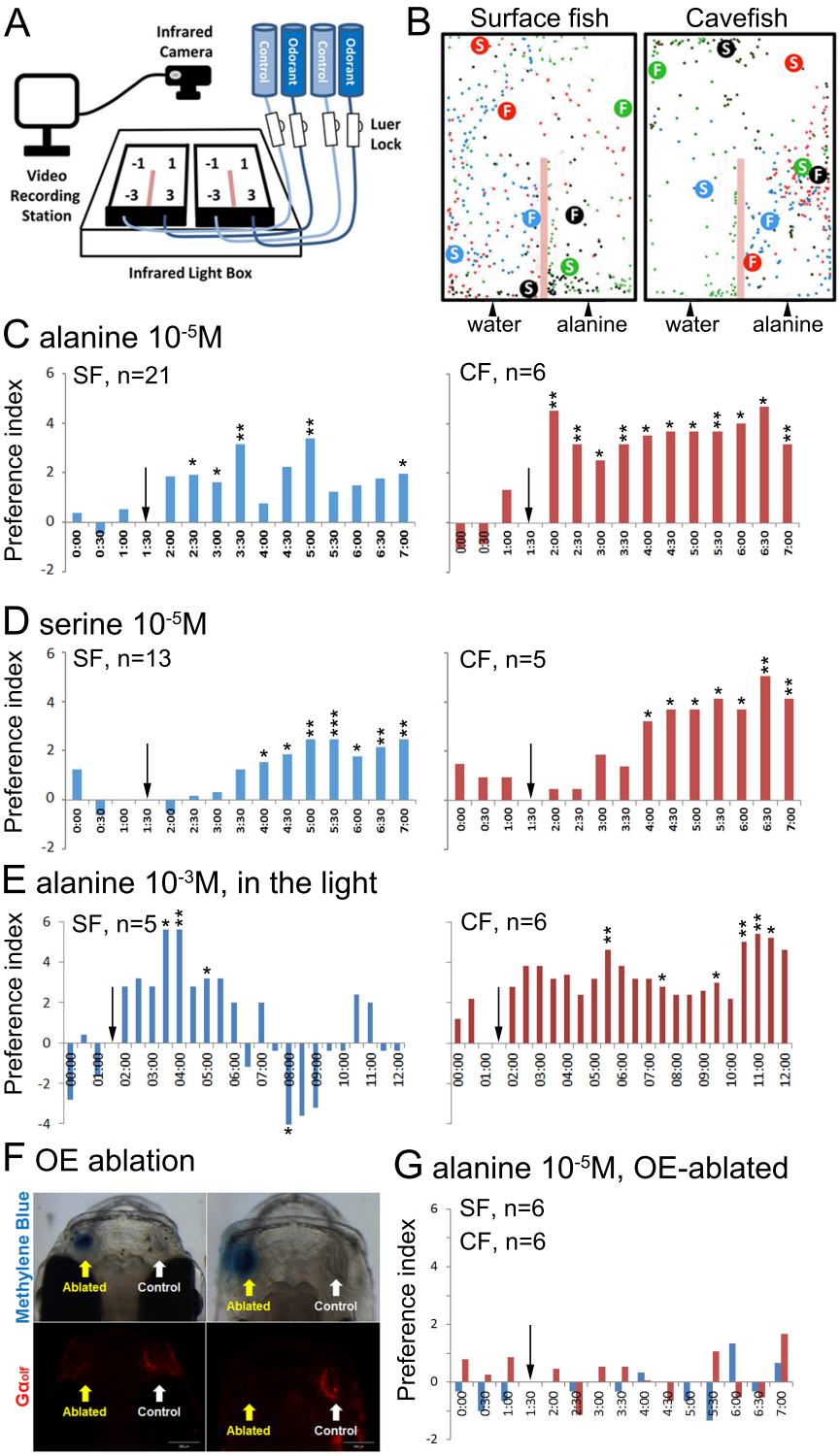

Fig. 7. Olfactory response to amino acids.
(A) Behavioral testing set-up. (B) Example of tracking for 1 µM alanine. The position of the four SF (left) or the four CF (right) was noted every 5 s during the test (colored dots). The four different colors follow the four fish in each box, with the start (S) position and the final (F) position indicated for each fish (see also Movie 1). (C,D) Response to 10 µM alanine (C) and 10 µM serine (D). The response to odorant is represented as the preference index as a function of time. Positive values indicate attraction. The arrow indicates the time when the odorant reaches the box. The conditions and number of tests are indicated (*n*=1 corresponds to one test, i.e. the cumulative score of four fish). Asterisks indicate significant response as compared with zero (Mann–Whitney): **P*<0.05, ***P*<0.01, ****P*<0.001. (E) Response to 1 mM alanine in the light during 12 min. (F) Superficial ablation of the OE by Triton X-100 application onto the olfactory cup. Top row illustrates the procedure, with the right side serving as control. Bottom row shows $G_{\alpha olf}$ immunofluorescence (red), which disappears on the ablated side. (G) OE-ablated SF and CF do not respond to 10 µM alanine.

It seems relevant to CF evolution and adaptation that its olfactory placode is enlarged. In the wild, in the Subterráneo cave (and hence a different CF population to the Pachón used here), adult CF have large nostrils and better chemosensory capabilities than non-troglomorphic fish (Bibliowicz et al., 2013). Here, we show that Pachón juveniles also possess large OEs and outstanding olfactory skills, demonstrating a case of parallel developmental and sensory evolution in two independently evolved CF populations (Bradic et al., 2012). Remarkably, only sharks have been reported to present such sensitivity (low response threshold) to amino acids with, for example, 10^{-11} M alanine eliciting electro-olfactogram responses in the hammerhead shark (Tricas et al., 2009). Although we cannot yet conclude that the difference in olfactory skills of CF and SF is entirely attributable to the difference in olfactory organ size, it is tempting to speculate that it at least in part stems from their developmentally controlled olfactory specialization.

In CF, the increase in olfactory placode size parallels the decrease in lens placode size, suggesting a developmental sensory trade-off: (1) in terms of patterning, the presumptive lens placode territory is reduced anteriorly, at a position that corresponds to the presumptive

Development (2016) 143, 4521-4532 doi:10.1242/dev.141291

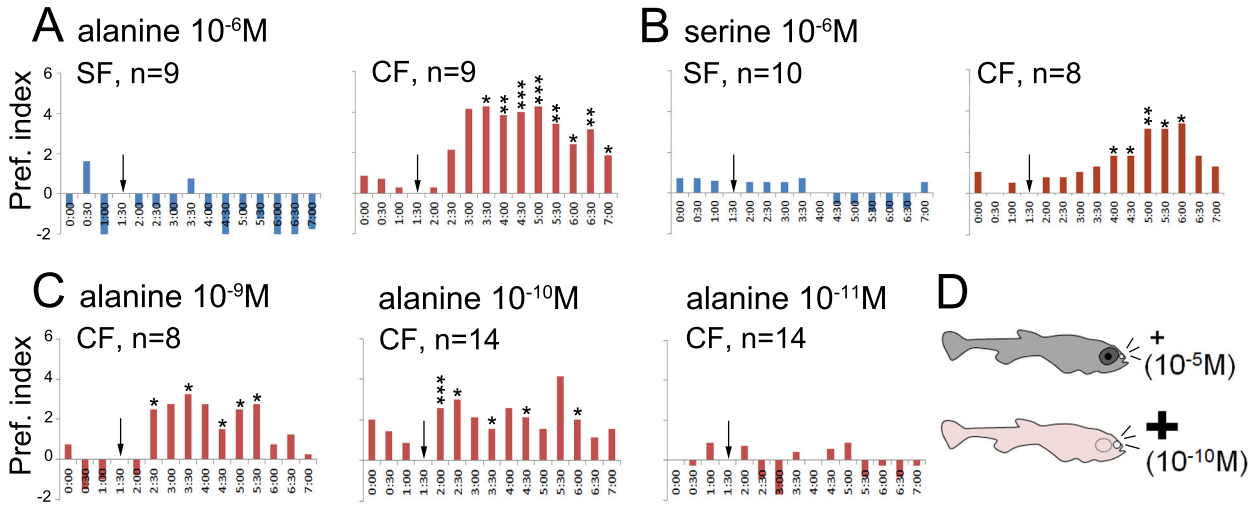

Fig. 8. Olfactory response thresholds in SF and CF. (A-C) Responses of SF and CF to decreasing concentrations of alanine (A,C) and serine (B). CF still respond to 0.1 µM serine (not shown), and therefore CF threshold for this amino acid is at least 0.1 µM. **P*<0.05, ***P*<0.01, ****P*<0.001, Mann–Whitney test. (D) Summary of the differences in olfactory anatomy and skills between SF (top) and CF (bottom).

territory of olfactory precursors according to zebrafish fate maps (Dutta et al., 2005; Toro and Varga, 2007); (2) the experimental manipulation of both Shh and Bmp4 signaling results in concomitant and opposite changes in the size of their lens/olfactory placodes. Together with the case of the gustatory/visual trade-off previously described (Yamamoto et al., 2009), these constitute the only examples to date of a direct link between the development of two sensory organs, involving a pleiotropic effect of these signaling systems, and suggesting indirect selection as an evolutionary driving force underlying the loss of eyes in CF (Jeffery, 2010; Retaux and Casane, 2013). In F2 hybrids, however, we did not observe an inverse correlation between lens and OE size, further suggesting that the developmental trade-off has a multigenic determinism.

We also found that *Bmp4* expression and signaling in the pcp are modified in CF compared with SF embryos (Fig. 4). Although several lines of evidence (*Pitx1* or *Gsc* expression) suggest that there is not a problem with migration of the CF pcp, we cannot exclude differences in cell movements between the two morphs. The dynamics of *Bmp4* expression are altered, whereas the total level of *Bmp4* expression at 10 hpf appears unchanged (Gross et al., 2016). Taking SF as 'wild type' and CF as 'mutant', an interpretation of the expression patterns would be the following: in SF, *Bmp4* is first turned on in the polster before 9.5 hpf and then in the ppcp; in CF, *Bmp4* expression would be turned off prematurely in the polster. Of note, the polster gives rise to the hatching gland, which develops and functions properly in CF [e.g. *Pitx1* expression in Figs S3 and 4; *Agr2* expression (Pottin et al., 2010); hatching time (Hinaux et al., 2011)]. Therefore, the modification in *Bmp4* expression dynamics in CF has no deleterious consequences on polster function, but does influence anterior neural development, as demonstrated by the Bmp4 injection experiments. Coupled with the previously described *Shh* heterotopy in the notochord and ppcp (Pottin et al., 2011; Yamamoto et al., 2004) and to the *Fgf8* heterochrony in the anterior neural territory (Pottin et al., 2011), our data on pcp *Bmp4* expression dynamics substantiate that three major signaling systems and organizer centers that orchestrate forebrain and head morphogenesis are altered in CF. Interestingly, *Bmp4* is found in QTL intervals controlling eye size (Borowsky and Cohen, 2013; Gross et al., 2008; Protas et al., 2007) and craniofacial bone fragmentation (Gross et al., 2016).

General considerations of sensory development and evolution

The data obtained from studies in model organisms on the roles of signaling systems in sensory placode development are sometimes contradictory (reviewed by Saint-Jeannet and Moody, 2014), perhaps owing to the fact that activation of similar combinations of signaling molecules at different time points can result in strikingly different outcomes (Lleras-Forero and Streit, 2012; Sjödal et al., 2007). Here, we studied three signaling systems in two morphs of a single species, and investigated their effects on the specification of regional placodal identity and sensory fate at the end of gastrulation/neural plate stage (Fig. 5F,G). In agreement with a stimulatory role of anterior neural ridge-derived Fgf8 signaling at neural fold stage in olfactory fate in chick (Bailey et al., 2006) and an inhibitory role of Shh in lens fate in zebrafish (Barth and Wilson, 1995; Dutta et al., 2005; Karlstrom et al., 1999; Kondoh et al., 2000; Varga et al., 2001), we found that Fgf8 heterochrony and Shh hyper-signaling at the anterior midline are responsible for the enlargement of the olfactory placode and the reduction of the lens placode territory in CF. Experiments performed in chick (Bailey et al., 2006) and Fgfr expression in zebrafish (ZFIN, *fgfr1a/fgfr1b* expression data) support a potential direct effect of Fgf signaling on the placodal region. Our results on CF, in which the difference with SF in terms of Fgf8 signaling comprises a 1.5 h expression heterochrony at the anterior neural border, points to the importance of the timing of Fgf8 signaling on placodal tissue [of note, *Fgf3* expression is unchanged in CF (Pottin et al., 2011)]. Conversely, Shh signaling effects on the lens and olfactory placode are probably indirect (Dutta et al., 2005), possibly via Fgf8 in the case of the olfactory placode (Pottin et al., 2011).

We also propose that Bmp4, as a signaling molecule secreted from the pcp as a signaling center, may influence placodal cell fate (Fig. 5F,G). This finding is distinct from the well-established early role of Bmp signaling in the specification of the neural plate border region/preplacodal region, which involves Bmp2/4/7 activity from the ventral side of the embryo at late blastula stages and the subsequent inhibition of Bmp signaling from the epidermis by Bmp inhibitors during gastrulation (Ahrens and Schlosser, 2005; Kwon et al., 2010; Nguyen et al., 1998; Reichert et al., 2013; Saint-Jeannet and Moody, 2014). In chick, a direct role for Bmp signaling in

Development (2016) 143, 4521-4532 doi:10.1242/dev.141291

placodal precursor specification at late gastrula stage, as well as a role for the time of Bmp exposure in the decision to follow a lens versus an olfactory fate, have been described (Sjödal et al., 2007). Our comparative approach using CF and SF have revealed a difference in Bmp4 expression dynamics in the pcp. This result and the functional experiments employing local Bmp4 injections at 10 hpf suggest that the timing of Bmp4 signaling from the pcp might be an important cue for lens fate specification, and support a general negative effect of sustained Bmp4 anterior midline signaling on olfactory fate. Our findings are also consistent with *Bmp4*$^{-/-}$ mice having normal olfactory derivatives but lacking lenses, although their placodal progenitors are initially correctly specified (Furuta and Hogan, 1998). Finally, the CF Bmp4 phenotype is not fully penetrant (Fig. 4). This might result from a polymorphism that is not fixed in CF. Yet, all CF have smaller lenses, probably because other pathways (Hh, Fgf, and perhaps others yet to be discovered) still contribute to size control, regardless of the Bmp4 phenotype.

Finally, our results concerning the pituitary are surprising. As Shh signaling is a potent inducer of pituitary fate (Dutta et al., 2005; Herzog et al., 2004; Karlstrom et al., 1999; Kondoh et al., 2000; Treier et al., 2001; Varga et al., 2001), one could expect to find a large adenohypophysis in CF with Shh hyper-signaling (Yamamoto et al., 2004). This was not the case. Indirectly, this suggests that other signaling modifications might compensate for Shh hyper-signaling in CF, and points to a possible negative control of pituitary fate in the placode by Fgf8 from the anterior neural ridge and Bmp4 from the pcp.

Conclusions

None of our experimental treatments led to full 'recovery' of CF lens to a size comparable to that of the SF lens. This is probably due to the fact that both Shh hyper-signaling from the ventral midline and lack of Bmp4 signal from the pcp are responsible for the small lens size in CF (Fig. 5F,G). Conversely, inhibition of either Shh or Fgf signaling in CF resulted in an olfactory placode identical in size to that of SF embryos. This shows the importance of Fgf8 and the associated Fgf8/Shh autoregulatory loop in the control of olfactory fate. These observations illuminate the subtle equilibrium that must exist in space and time between the signaling systems to orchestrate the development of the surrounding sensory epithelium. In model species, manipulation of early signaling systems usually results in 'monstrous' phenotypes. It might thus seem doubtful that morphological evolution is due to modifications at this level. However, we show that subtle changes in the equilibrium between signaling systems at the end of gastrulation can participate in natural morphological evolution, and are part of the developmental evolutionary toolkit. Here, we have deciphered the impact of fine changes in the strength or timing of three signaling pathways emanating from three organizer centers in the developmental evolution of sensory systems in *Astyanax*. As we have studied the CF 'natural mutant', an animal that is viable and adapted to its environment, the early developmental mechanisms that we have uncovered are probably generally applicable and relevant to adaptive sensory evolution and specialization in vertebrates.

MATERIALS AND METHODS

Animals

Laboratory stocks of *A. mexicanus* SF and Pachón CF were obtained in 2004 from the Jeffery laboratory at the University of Maryland and maintained as previously described (Elipot et al., 2014). Embryos were collected after natural spawning, grown at 23°C, staged according to the developmental staging table (Hinaux et al., 2011) and fixed in 4% paraformaldehyde. After progressive dehydration in methanol, they were stored at –20°C.

Animals were treated according to French and European regulations for handling of animals in research. S.R.'s authorization for use of animals in research is 91-116, and Paris Centre-Sud Ethic Committee authorization numbers are 2012-0052 and 2012-0055.

Lens and OE measurements

F1 hybrid larvae were obtained by *in vitro* fertilization of female SF eggs by Pachón male sperm (Elipot et al., 2014). They were photographed at 36 hpf under an Olympus SZX16 stereomicroscope. Measurements were made on the images using ImageJ software (NIH).

F2 larvae were fixed and immediately double stained with DAPI and DiI and imaged under an SP8 confocal microscope (Leica). Lens and OE volumes were measured with Fiji using the MeasureStack plugin.

cDNA cloning

Total RNA from *Astyanax* embryos of various stages (6-36 hpf) was reverse-transcribed using the iScript cDNA synthesis kit (Bio-Rad). Partial cDNA sequences for *Omp* (GenBank ID KP826791.1), *Lhx3* (KP826792.1), *Pitx1* (KP826793.1) and *Pitx2* (KP826794.1) were amplified by PCR (for primers, see the supplementary Materials and Methods) and subcloned in the TOPO-PCR II vector (Invitrogen). *Zic1* (FO290256) and *Eya2* (FO211529) partial cDNAs originate from our cDNA library (Hinaux et al., 2013). Phylogenetic analyses (Figs S8-S12) were conducted to determine orthology relationships. Deuterostomes sequences were retrieved from the Ensembl database based on their annotation, aligned using MAFFT v7.023b (http://mafft.cbrc.jp/alignment/software/) with manual correction. Maximum likelihood analyses were performed using PhyML (Guindon and Gascuel, 2003), with the LG model of amino acid substitution and a BioNJ tree as the input tree. A gamma distribution with four discrete categories was used. The gamma shape parameter and the proportion of invariant sites were optimized during the searches. The statistical significance of the nodes was assessed by bootstrapping (100 replicates). *Shh* (AY661431), *Pax6* (AY651762.1) and *Bmp4* (DQ915173) cDNA were isolated previously.

In situ hybridization

Digoxygenin-labeled riboprobes were synthesized from PCR templates. A protocol for automated whole-mount *in situ* hybridization (Intavis) was used (Deyts et al., 2005). Embryos were photographed *in toto* under a Nikon AZ100 stereomicroscope using agarose wells. Some were embedded in paraffin, sectioned (8 µm) and counterstained, using Prolong Gold anti-fade with DAPI (Invitrogen).

For fluorescent double *in situ* hybridization, Cy3- and FITC-tyramides were prepared and embryos were processed as previously described (Zhou and Vize, 2004; Pottin et al., 2011). Embryos were imaged with either an Olympus SZX16 stereomicroscope, a Zeiss Apotome or a Nikon Eclipse E800 microscope.

Immunohistochemistry

Whole-mount immunofluorescence was performed using $G_{\alpha olf}$ primary antibody (Santa Cruz Biotechnology, sc-383; 1/1000) and Alexa Fluor secondary antibodies (Invitrogen, A-11008 and A-11037; 1/500). Samples were imaged using an Olympus SZX16 microscope. Size measurements were performed on images using ImageJ.

Pharmacological treatments

Manually dechorionated CF embryos were incubated in 100 µM cyclopamine (C-8700, LC Laboratories) or 0.5 µM SU5402 (215543-92-3, Calbiochem) diluted in blue water (Elipot et al., 2014) from 6 to 10 hpf. Controls were incubated in an equivalent concentration of ethanol or DMSO, respectively. They were washed in blue water and fixed at 16 hpf or 28 hpf. To define and ascertain the working concentrations of cyclopamine and SU5402, we checked that hatched larvae have a typical 'comma shape' or tail bud defects, respectively.

Bmp4 protein microinjection

CF and SF embryos at 10 hpf were placed in agarose wells under an Olympus SZX12 stereomicroscope equipped with a micromanipulator.

Development (2016) 143, 4521-4532 doi:10.1242/dev.141291

They were micro-injected with a solution of 0.1 µg/µl Bmp4 protein (R&D Systems), 10% glycerol in Phenol Red/water, either anteriorly to the polster region or under the notochord, posterior to the head. Embryos were photographed under an Olympus SZX16 stereomicroscope and sorted according to the precise region of injection (marked by Phenol Red). They were fixed at 16 hpf or 28 hpf.

Behavioral testing

Four juveniles were placed in each of two behavioral testing boxes positioned on an infrared light source (ViewPoint). They were acclimatized for 2 h in the dark. Perfusion of the amino acid and control solution was initiated simultaneously as recordings started (Dragonfly2 camera, ViewPoint imaging software). A preference index score was calculated for each fish every 30 s, depending on its position relative to the amino acid source: +3 for the quadrant closest to the source, with +1, −1, −3 for the quadrants progressively further from the source (Fig. 7A; supplementary Materials and Methods). This score was then corrected for the position of the fish when the amino acid reached the box at 1.5 min after perfusion opening.

OE ablation

Ablation of the OE was adapted from Iqbal and Byrd-Jacobs (2010). One-month-old fish were anesthetized using 0.1% MS-222 (Sigma) in embryo medium (EM) and chemical ablation of each naris was performed using a solution of 0.05% Methylene Blue, 0.7% Triton X-100 in EM perfused continuously with a micro-injector (Eppendorf, Femtojet) for 90 s. After ablation, fish were allowed to recover for 24 h before being used for behavioral tests or fixed for immunohistochemistry.

Acknowledgements

We thank Stéphane Père and Diane Denis for *Astyanax* care; Laurent Legendre and Victor Simon for obtaining hybrids.

Competing interests

The authors declare no competing or financial interests.

Author contributions

H.H. and S.R. conceived and analyzed embryology experiments; H.H. performed the experiments with help from L.D. and M.B.; S.R., Y.E., J.B. and M.B. conceived and performed the behavior experiments; A.A. performed phylogenetic analyses; S.R. and H.H. wrote the paper.

Funding

This work was supported by Agence Nationale de la Recherche (ANR) grants (ASTYCO and BLINDTEST), a Fondation pour la Recherche Médicale (FRM) grant (Equipe FRM) and Centre National de la Recherche Scientifique (CNR) to S.R. H.H. was supported by Retina France and ANR; Y.B. by ANR and an FRM postdoctoral fellowship; and Y.E. by an FRM Engineer grant.

Data availability

The partial cDNA sequences for Astyanax mexicanus OMP (accession number KP826791.1), *Lhx3* (KP826792.1), *Pitx1* (KP826793.1) and *Pitx2* (KP826794.1) are available at GenBank.

Supplementary information

Supplementary information available online at
http://dev.biologists.org/lookup/doi/10.1242/dev.141291.supplemental

References

Ahrens, K. and Schlosser, G. (2005). Tissues and signals involved in the induction of placodal Six1 expression in Xenopus laevis. *Dev. Biol.* **288**, 40-59.

Alunni, A., Menuet, A., Candal, E., Pénigault, J.-B., Jeffery, W. R. and Rétaux, S. (2007). Developmental mechanisms for retinal degeneration in the blind cavefish Astyanax mexicanus. *J. Comp. Neurol.* **505**, 221-233.

Bailey, A. P. and Streit, A. (2006). Sensory organs: making and breaking the pre-placodal region. *Curr. Top. Dev. Biol.* **72**, 167-204.

Bailey, A. P., Bhattacharyya, S., Bronner-Fraser, M. and Streit, A. (2006). Lens specification is the ground state of all sensory placodes, from which FGF promotes olfactory identity. *Dev. Cell* **11**, 505-517.

Barth, K. A. and Wilson, S. W. (1995). Expression of zebrafish nk2.2 is influenced by sonic hedgehog/vertebrate hedgehog-1 and demarcates a zone of neuronal differentiation in the embryonic forebrain. *Development* **121**, 1755-1768.

Behrens, M., Wilkens, H. and Schmale, H. (1998). Cloning of the alphaA-crystallin genes of a blind cave form and the epigean form of Astyanax fasciatus: a comparative analysis of structure, expression and evolutionary conservation. *Gene* **216**, 319-326.

Bibliowicz, J., Alié, A., Espinasa, L., Yoshizawa, M., Blin, M., Hinaux, H., Legendre, L., Père, S. and Rétaux, S. (2013). Differences in chemosensory response between eyed and eyeless Astyanax mexicanus of the Rio Subterraneo cave. *EvoDevo* **4**, 25.

Borowsky, R. and Cohen, D. (2013). Genomic consequences of ecological speciation in astyanax cavefish. *PLoS ONE* **8**, e79903.

Bradic, M., Beerli, P., García-de León, F. J., Esquivel-Bobadilla, S. and Borowsky, R. L. (2012). Gene flow and population structure in the Mexican blind cavefish complex (Astyanax mexicanus). *BMC Evol. Biol.* **12**, 9.

Byrd, R. P., Jr and Caprio, J. (1982). Comparison of olfactory receptor (EOG) and bulbar (EEG) responses to amino acids in the catfish, Ictalurus punctatus. *Brain Res.* **249**, 73-80.

Campi, K. L. and Krubitzer, L. (2010). Comparative studies of diurnal and nocturnal rodents: differences in lifestyle result in alterations in cortical field size and number. *J. Comp. Neurol.* **518**, 4491-4512.

Chen, J. K., Taipale, J., Cooper, M. K. and Beachy, P. A. (2002). Inhibition of Hedgehog signaling by direct binding of cyclopamine to Smoothened. *Genes Dev.* **16**, 2743-2748.

Collin, S. P. (2012). The neuroecology of cartilaginous fishes: sensory strategies for survival. *Brain Behav. Evol.* **80**, 80-96.

Crish, S. D., Rice, F. L., Park, T. J. and Comer, C. M. (2003). Somatosensory organization and behavior in naked mole-rats I: vibrissa-like body hairs comprise a sensory array that mediates orientation to tactile stimuli. *Brain Behav. Evol.* **62**, 141-151.

Derby, C. D. and Sorensen, P. W. (2008). Neural processing, perception, and behavioral responses to natural chemical stimuli by fish and crustaceans. *J. Chem. Ecol.* **34**, 898-914.

Deyts, C., Candal, E., Joly, J. S. and Bourrat, F. (2005). An automated in situ hybridization screen in the medaka to identify unknown neural genes. *Dev. Dyn.* **3**, 698-708.

Dolensek, J. and Valentincic, T. (2010). Specificities of olfactory receptor neuron responses to amino acids in the black bullhead catfish (Ameiurus melas). *Pflugers Arch.* **459**, 413-425.

Dutta, S., Dietrich, J.-E., Aspöck, G., Burdine, R. D., Schier, A., Westerfield, M. and Varga, Z. M. (2005). pitx3 defines an equivalence domain for lens and anterior pituitary placode. *Development* **132**, 1579-1590.

Elipot, Y., Legendre, L., Père, S., Sohm, F. and Rétaux, S. (2014). Astyanax transgenesis and husbandry: how cavefish enters the lab. *Zebrafish* **11**, 291-299.

Espinasa, L., Bibliowicz, J., Jeffery, W. R. and Retaux, S. (2014). Enhanced prey capture skills in Astyanax cavefish larvae are independent from eye loss. *Evodevo* **5**, 35.

Evans, R. E. and Hara, T. J. (1985). The characteristics of the electro-olfactogram (EOG): its loss and recovery following olfactory nerve section in rainbow trout (Salmo gairdneri). *Brain Res.* **330**, 65-75.

Franz-Odendaal, T. A. and Hall, B. K. (2006). Modularity and sense organs in the blind cavefish, Astyanax mexicanus. *Evol. Dev.* **8**, 94-100.

Friedrich, R. W. and Korsching, S. I. (1997). Combinatorial and chemotopic odorant coding in the zebrafish olfactory bulb visualized by optical imaging. *Neuron* **18**, 737-752.

Furuta, Y. and Hogan, B. L. M. (1998). BMP4 is essential for lens induction in the mouse embryo. *Genes Dev.* **12**, 3764-3775.

Gross, J. B., Protas, M., Conrad, M., Scheid, P. E., Vidal, O., Jeffery, W. R., Borowsky, R. and Tabin, C. J. (2008). Synteny and candidate gene prediction using an anchored linkage map of Astyanax mexicanus. *Proc. Natl. Acad. Sci. USA* **105**, 20106-20111.

Gross, J. B., Stahl, B. A., Powers, A. K. and Carlson, B. M. (2016). Natural bone fragmentation in the blind cave-dwelling fish, Astyanax mexicanus: candidate gene identification through integrative comparative genomics. *Evol. Dev.* **18**, 7-18.

Guindon, S. and Gascuel, O. (2003). A simple, fast, and accurate algorithm to estimate large phylogenies by maximum likelihood. *Syst. Biol.* **52**, 696-704.

Hansen, A., Anderson, K. T. and Finger, T. E. (2004). Differential distribution of olfactory receptor neurons in goldfish: structural and molecular correlates. *J. Comp. Neurol.* **477**, 347-359.

Hara, T. J. (1994). Olfaction and gustation in fish: an overview. *Acta Physiol. Scand.* **152**, 207-217.

Hara, T. J. (2006). Feeding behaviour in some teleosts is triggered by single amino acids primarily through olfaction. *J. Fish Biol.* **68**, 810-825.

Hara, T. J. (2015). Taste in aquatic vertebrates. In *Handbook of Olfaction and Gustation*, Chapter 42, 3rd Edn. (ed. R. L. Doty), pp. 949-958. Chichester: Wiley-Blackwell.

Herzog, W., Sonntag, C., von der Hardt, S., Roehl, H. H., Varga, Z. M. and Hammerschmidt, M. (2004). Fgf3 signaling from the ventral diencephalon is required for early specification and subsequent survival of the zebrafish adenohypophysis. *Development* **131**, 3681-3692.

Hinaux, H., Pottin, K., Chalhoub, H., Père, S., Elipot, Y., Legendre, L. and Rétaux, S. (2011). A developmental staging table for Astyanax mexicanus surface fish and Pachon cavefish. *Zebrafish* **8**, 155-165.
Hinaux, H., Poulain, J., Da Silva, C., Noirot, C., Jeffery, W. R., Casane, D. and Rétaux, S. (2013). De Novo sequencing of Astyanax mexicanus surface fish and Pachon cavefish transcriptomes reveals enrichment of mutations in cavefish putative eye genes. *PLoS ONE* **8**, e53553.
Hinaux, H., Blin, M., Fumey, J., Legendre, L., Heuze, A., Casane, D. and Retaux, S. (2014). Lens defects in Astyanax mexicanus Cavefish: evolution of crystallins and a role for alphaA-crystallin. *Dev. Neurobiol.* **75**, 505-521.
Hüppop, K. (1987). Food-finding ability in cave fish (Astyanax fasciatus). *Int. J. Speleol.* **16**, 59-66.
Iqbal, T. and Byrd-Jacobs, C. (2010). Rapid degeneration and regeneration of the zebrafish olfactory epithelium after Triton X-100 application. *Chem. Senses* **35**, 351-361.
Jeffery, W. R. (2008). Emerging model systems in evo-devo: cavefish and microevolution of development. *Evol. Dev.* **10**, 265-272.
Jeffery, W. R. (2009). Evolution and development in the cavefish Astyanax. *Curr. Top. Dev. Biol.* **86**, 191-221.
Jeffery, W. R. (2010). Pleiotropy and eye degeneration in cavefish. *Heredity (Edin.)* **105**, 495-496.
Jeffery, W. R., Strickler, A. G., Guiney, S., Heyser, D. G. and Tomarev, S. I. (2000). Prox 1 in eye degeneration and sensory organ compensation during development and evolution of the cavefish Astyanax. *Dev. Genes Evol.* **210**, 223-230.
Karlstrom, R. O., Talbot, W. S. and Schier, A. F. (1999). Comparative synteny cloning of zebrafish you-too: mutations in the Hedgehog target gli2 affect ventral forebrain patterning. *Genes Dev.* **13**, 388-393.
Kiecker, C. and Niehrs, C. (2001). The role of prechordal mesendoderm in neural patterning. *Curr. Opin. Neurobiol.* **11**, 27-33.
Koide, T., Miyasaka, N., Morimoto, K., Asakawa, K., Urasaki, A., Kawakami, K. and Yoshihara, Y. (2009). Olfactory neural circuitry for attraction to amino acids revealed by transposon-mediated gene trap approach in zebrafish. *Proc. Natl. Acad. Sci. USA* **106**, 9884-9889.
Kondoh, H., Uchikawa, M., Yoda, H., Takeda, H., Furutani-Seiki, M. and Karlstrom, R. O. (2000). Zebrafish mutations in Gli-mediated hedgehog signaling lead to lens transdifferentiation from the adenohypophysis anlage. *Mech. Dev.* **96**, 165-174.
Korsching, S. I., Argo, S., Campenhausen, H., Friedrich, R. W., Rummrich, A. and Weth, F. (1997). Olfaction in zebrafish: what does a tiny teleost tell us? *Semin. Cell Dev. Biol.* **8**, 181-187.
Krubitzer, L., Campi, K. L. and Cooke, D. F. (2011). All rodents are not the same: a modern synthesis of cortical organization. *Brain Behav. Evol.* **78**, 51-93.
Kwon, H.-J., Bhat, N., Sweet, E. M., Cornell, R. A. and Riley, B. B. (2010). Identification of early requirements for preplacodal ectoderm and sensory organ development. *PLoS Genet.* **6**, e1001133.
Lindsay, S. M. and Vogt, R. G. (2004). Behavioral responses of newly hatched zebrafish (Danio rerio) to amino acid chemostimulants. *Chem. Senses* **29**, 93-100.
Lleras-Forero, L. and Streit, A. (2012). Development of the sensory nervous system in the vertebrate head: the importance of being on time. *Curr. Opin. Genet. Dev.* **22**, 315-322.
Ma, L., Parkhurst, A. and Jeffery, W. R. (2014). The role of a lens survival pathway including sox2 and alphaA-crystallin in the evolution of cavefish eye degeneration. *Evodevo* **5**, 28.
Martin, K. and Groves, A. K. (2006). Competence of cranial ectoderm to respond to Fgf signaling suggests a two-step model of otic placode induction. *Development* **133**, 877-887.
Menuet, A., Alunni, A., Joly, J.-S., Jeffery, W. R. and Retaux, S. (2007). Expanded expression of Sonic Hedgehog in Astyanax cavefish: multiple consequences on forebrain development and evolution. *Development* **134**, 845-855.
Mohammadi, M., McMahon, G., Sun, L., Tang, C., Hirth, P., Yeh, B. K., Hubbard, S. R. and Schlessinger, J. (1997). Structures of the tyrosine kinase domain of fibroblast growth factor receptor in complex with inhibitors. *Science* **276**, 955-960.
Nguyen, V. H., Schmid, B., Trout, J., Connors, S. A., Ekker, M. and Mullins, M. C. (1998). Ventral and lateral regions of the zebrafish gastrula, including the neural crest progenitors, are established by a bmp2b/swirl pathway of genes. *Dev. Biol.* **199**, 93-110.
Nummela, S., Pihlström, H., Puolamäki, K., Fortelius, M., Hemilä, S. and Reuter, T. (2013). Exploring the mammalian sensory space: co-operations and trade-offs among senses. *J. Comp. Physiol. A Neuroethol. Sens. Neural Behav. Physiol.* **199**, 1077-1092.
Park, T. J., Comer, C., Carol, A., Lu, Y., Hong, H. S. and Rice, F. L. (2003). Somatosensory organization and behavior in naked mole-rats: II. Peripheral structures, innervation, and selective lack of neuropeptides associated with thermoregulation and pain. *J. Comp. Neurol.* **465**, 104-120.
Pollen, A. A., Dobberfuhl, A. P., Scace, J., Igulu, M. M., Renn, S. C. P., Shumway, C. A. and Hofmann, H. A. (2007). Environmental complexity and social organization sculpt the brain in Lake Tanganyikan cichlid fish. *Brain Behav. Evol.* **70**, 21-39.
Pottin, K., Hyacinthe, C. and Retaux, S. (2010). Conservation, development, and function of a cement gland-like structure in the fish Astyanax mexicanus. *Proc. Natl. Acad. Sci. USA* **107**, 17256-17261.
Pottin, K., Hinaux, H. and Retaux, S. (2011). Restoring eye size in Astyanax mexicanus blind cavefish embryos through modulation of the Shh and Fgf8 forebrain organising centres. *Development* **138**, 2467-2476.
Protas, M., Conrad, M., Gross, J. B., Tabin, C. and Borowsky, R. (2007). Regressive evolution in the Mexican cave tetra, Astyanax mexicanus. *Curr. Biol.* **17**, 452-454.
Protas, M., Tabansky, I., Conrad, M., Gross, J. B., Vidal, O., Tabin, C. J. and Borowsky, R. (2008). Multi-trait evolution in a cave fish, Astyanax mexicanus. *Evol. Dev.* **10**, 196-209.
Reichert, S., Randall, R. A. and Hill, C. S. (2013). A BMP regulatory network controls ectodermal cell fate decisions at the neural plate border. *Development* **140**, 4435-4444.
Retaux, S. and Casane, D. (2013). Evolution of eye development in the darkness of caves: adaptation, drift, or both? *Evodevo* **4**, 26.
Riedel, G. and Krug, L. (1997). The forebrain of the blind cave fish Astyanax hubbsi (Characidae). II. Projections of the olfactory bulb. *Brain Behav. Evol.* **49**, 39-52.
Saint-Jeannet, J.-P. and Moody, S. A. (2014). Establishing the pre-placodal region and breaking it into placodes with distinct identities. *Dev. Biol.* **389**, 13-27.
Sarko, D. K., Rice, F. L. and Reep, R. L. (2011). Mammalian tactile hair: divergence from a limited distribution. *Ann. N. Y. Acad. Sci.* **1225**, 90-100.
Schemmel, C. (1967). Vergleichende Untersuchungen an den Hautsinnesorganen ober-and unter-irdisch lebender Astyanax-Foramen. *Z. Morph. Tiere.* **61**, 255-316.
Schlosser, G. (2006). Induction and specification of cranial placodes. *Dev. Biol.* **294**, 303-351.
Sjödal, M., Edlund, T. and Gunhaga, L. (2007). Time of exposure to Bmp signals play a key role in the specification of the olfactory and lens placodes ex vivo. *Dev. Cell* **13**, 141-149.
Streit, A. (2007). The preplacodal region: an ectodermal domain with multipotential progenitors that contribute to sense organs and cranial sensory ganglia. *Int. J. Dev. Biol.* **51**, 447-461.
Streit, A. (2008). *The Cranial Sensory Nervous System: Specification of Sensory Progenitors and Placodes*. *StemBook*, doi: 10.3824/stembook.1.31.1.
Strickler, A. G., Yamamoto, Y. and Jeffery, W. R. (2001). Early and late changes in Pax6 expression accompany eye degeneration during cavefish development. *Dev. Genes Evol.* **211**, 138-144.
Strickler, A. G., Byerly, M. S. and Jeffery, W. R. (2007). Lens gene expression analysis reveals downregulation of the anti-apoptotic chaperone alphaA-crystallin during cavefish eye degeneration. *Dev. Genes Evol.* **217**, 771-782.
Toro, S. and Varga, Z. M. (2007). Equivalent progenitor cells in the zebrafish anterior preplacodal field give rise to adenohypophysis, lens, and olfactory placodes. *Semin. Cell Dev. Biol.* **18**, 534-542.
Torres-Paz, J. and Whitlock, K. E. (2014). Olfactory sensory system develops from coordinated movements within the neural plate. *Dev. Dyn.* **243**, 1619-1631.
Treier, M., O'Connell, S., Gleiberman, A., Price, J., Szeto, D. P., Burgess, R., Chuang, P. T., McMahon, A. P. and Rosenfeld, M. G. (2001). Hedgehog signaling is required for pituitary gland development. *Development* **128**, 377-386.
Tricas, T. C., Kajiura, S. M. and Summers, A. P. (2009). Response of the hammerhead shark olfactory epithelium to amino acid stimuli. *J. Comp. Physiol. A Neuroethol. Sens. Neural Behav. Physiol.* **195**, 947-954.
Varatharasan, N., Croll, R. P. and Franz-Odendaal, T. (2009). Taste bud development and patterning in sighted and blind morphs of Astyanax mexicanus. *Dev. Dyn.* **238**, 3056-3064.
Varga, Z. M., Amores, A., Lewis, K. E., Yan, Y. L., Postlethwait, J. H., Eisen, J. S. and Westerfield, M. (2001). Zebrafish smoothened functions in ventral neural tube specification and axon tract formation. *Development* **128**, 3497-3509.
Vitebsky, A., Reyes, R., Sanderson, M. J., Michel, W. C. and Whitlock, K. E. (2005). Isolation and characterization of the laure olfactory behavioral mutant in the zebrafish, Danio rerio. *Dev. Dyn.* **234**, 229-242.
Wark, A. R. and Peichel, C. L. (2010). Lateral line diversity among ecologically divergent threespine stickleback populations. *J. Exp. Biol.* **213**, 108-117.
Wekesa, K. S. and Anholt, R. R. (1999). Differential expression of G proteins in the mouse olfactory system. *Brain Res.* **837**, 117-126.
Whitlock, K. E. and Westerfield, M. (2000). The olfactory placodes of the zebrafish form by convergence of cellular fields at the edge of the neural plate. *Development* **127**, 3645-3653.
Wilkens, H. (2010). Genes, modules and the evolution of cave fish. *Heredity (Edin.)* **105**, 413-422.
Yamamoto, Y. and Jeffery, W. R. (2000). Central role for the lens in cave fish eye degeneration. *Science* **289**, 631-633.
Yamamoto, Y., Espinasa, L., Stock, D. W. and Jeffery, W. R. (2003). Development and evolution of craniofacial patterning is mediated by eye-dependent and -independent processes in the cavefish Astyanax. *Evol. Dev.* **5**, 435-446.
Yamamoto, Y., Stock, D. W. and Jeffery, W. R. (2004). Hedgehog signalling controls eye degeneration in blind cavefish. *Nature* **431**, 844-847.

Development (2016) 143, 4521-4532 doi:10.1242/dev.141291

Yamamoto, Y., Byerly, M. S., Jackman, W. R. and Jeffery, W. R. (2009). Pleiotropic functions of embryonic sonic hedgehog expression link jaw and taste bud amplification with eye loss during cavefish evolution. *Dev. Biol.* **330**, 200-211.

Yoshizawa, M. and Jeffery, W. R. (2011). Evolutionary tuning of an adaptive behavior requires enhancement of the neuromast sensory system. *Commun. Integr. Biol.* **4**, 89-91.

Zhou, X. and Vize, P. D. (2004). Proximo-distal specialization of epithelial transport processes within the Xenopus pronephric kidney tubules. *Dev. Biol.* **271**, 322-338.

Supplemental Materials and Methods

Cloning primers:

Omp-Fw: TGCTACAGGGTCTAGGTCGTC;

Omp-Rv: GGCCTCGTTCTTCTTGAACATC;

Lhx3-Fw: CGGATCGAGTTGCCAGAACG;

Lhx3-Rv: CCTCCACCAACCATTCGCAC;

Pitx-Fw: GTKTGGTTCAARAACCGSMG;

Pitx1-Rv: TCARCTGTTRTACTGGCASGC;

Pitx2-Rv: CANGTGTCCCGGTANACGCTGTANGGRGA

Behavioral testing:

1) **Detailed protocols**

Behavioral tests were performed in a specially constructed sound- and light-proof room that includes a main compartment for testing and a second computer work station compartment from which recording of the tests was performed with minimal disturbances. All fish were fed exactly 24 hours prior to the test with two days-old artemia and then starved until testing in order to standardize their feeding state. Four juveniles (one-month-old; about 5-6 mm in length) were placed in each of two behavioral testing boxes (9 cm wide x 13 cm long) containing 150mL embryo medium (EM) and let acclimatize for two hours prior to the test at a temperature of 26-28°C in the dark (**Fig. 7A**). SF and CF (or experimental and control animals) were always tested in parallel. Boxes were placed on top of a custom-made 50x50cm infrared light box (ViewPoint S.A.). Each test was initiated by simultaneously opening the Luer stoppers of medical solution administration tubing (Baxter, U.K.) to perfuse solutions at

5mL/min from two reservoirs containing 60mL of either amino-acid containing EM or EM alone (control). On the control side, the flow generated was identical to the flow on the amino acid perfused side. Tests were recorded for 7 minutes on a Dell work station using ViewPoint imaging software and a DragonFly2 camera equipped with an infrared filter (PointGray).

Utilizing a colorimetric test for the quantification of amino acid concentrations, we determined that the amino acids reached the boxes 1.5 minutes after opening the perfusion system and we defined four quadrants of the boxes in which the amino acid concentration was very high, high, low or zero over the duration of the test (**Fig. S6 ABC**). Each of these quadrant was attributed a coefficient to calculate a Preference Index Score (PIS) reflecting the attraction of fish (or absence of attraction) to the amino acid source. The PIS for each time point (at 30 second intervals) was the cumulative score of the four fish in the box, where the position of each fish was scored with the values of -3 (quadrant furthest away from amino acid source), -1, 1, or 3 (quadrant closest to amino acid source). Thus the maximum and minimum PIS scores are +12 and -12, respectively, for a given time point. In order to correct for the initial position of the fish when the amino acid first enters the box at 1.5 minute, the PIS was reset at zero for this time point and the subsequent PIS values were corrected by subtracting the initial raw score at 1.5 minute. Experiments in which the initial PIS score was >6 or <-6 were discarded because the correction for initial position of the fish lead to artefactual “false attraction” or “false repulsion” at subsequent time points. Statistical significance of replicate tests was calculated using the non-parametric Mann-Whitney test, using the StatView software. In all figures, n=1 corresponds to one test, i.e., the cumulative score of 4 fish. Significance was set at $p<0.05$ (*). **, ***, and **** correspond to $p<0.01$, $p<0.001$, and $p<0.0001$, respectively.

In addition, individual fish were tracked manually during the olfaction behavior assay and the total distance swam during the 7 minutes test was calculated, to control for possible differences in exploratory behavior (**Fig. S6D**).

2) Colorimetric quantification of amino-acids in solution

The concentration of amino-acid in solution in the behavioral boxes was quantified using an adapted version of previously used methods (Friedman, 2004). Briefly, 4mL of amino-acid solution were added to 1mL of 8% Ninhydrin (Sigma-Aldrich) in acetone. The solution was heated in a water bath for 15min at 80°C and then immediately cooled on ice. 1mL of 50% EtOH was then added and solution mixed by inverting the tube. The samples were analyzed using a Biowave II spectrophotometer (WPA) at 570nm. Amino-acid concentrations were extrapolated using a standard curve obtained using solutions of known concentrations.

Supplemental material.

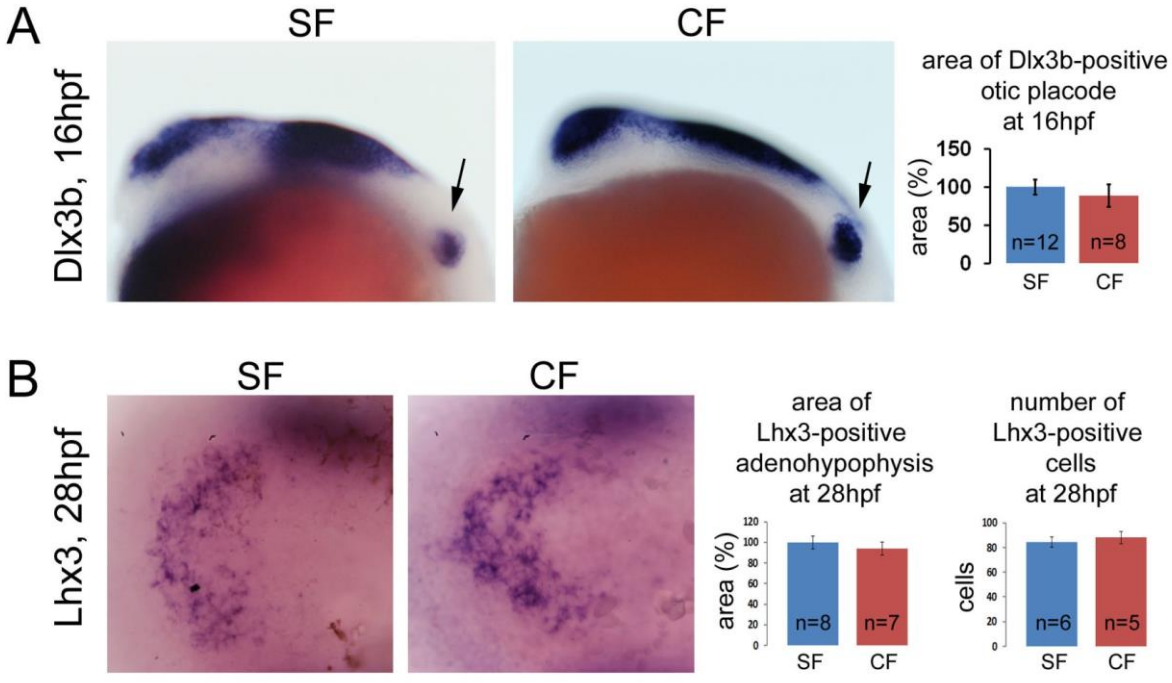

Suppl. Figure 1

Suppl. Figure 1: additional data on comparative patterning of the placodes.

A, At 16hpf, *Dlx3b* also labels the posterior otic placodes (arrows), seen here on lateral views. Measurements of the size of the *Dlx3b*-positive otic placodes in CF and SF show no significant size difference (NS, Mann Whitney test). Data are mean±s.e.m.

B, Ventral views of dissected brains at 28hpf after *Lhx3 in situ* hybridization. Neither measurements of the size of the *Lhx3*-positive adenohypophysis area nor counts of Lhx3-positive cells in CF and SF show significant difference (NS, Mann Whitney test). Data are mean±s.e.m.

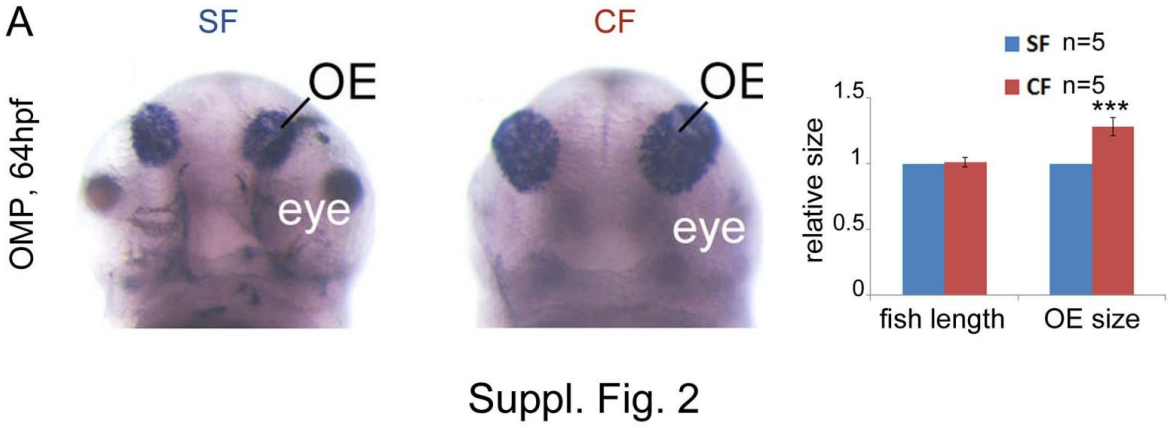

Suppl. Fig. 2

Suppl. Figure 2: additional data on olfactory placode size.

A, Photographs of 64hpf SF and CF after *in situ* hybridization for *OMP* in frontal views, and quantification of olfactory epithelium size.

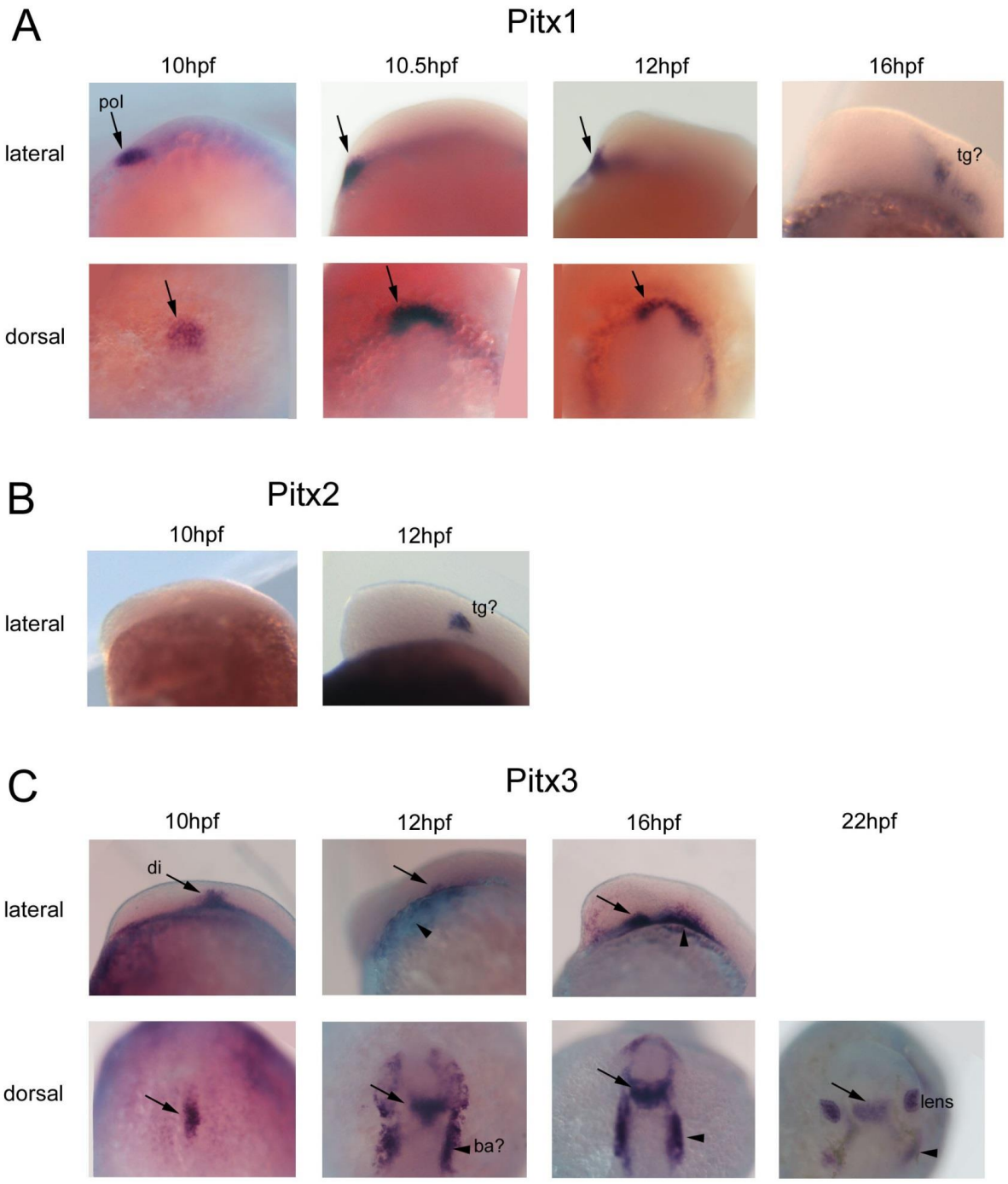

Suppl. Fig. 3

Suppl. Figure 3: additional data on *Pitx* genes expression time-courses.

Only SF embryos are shown. Expression patterns in CF are identical. The 3 *Pitx* genes analyzed are not expressed in the presumptive pituitary at the stages analyzed.

A, Time-course analysis of *Pitx1* expression between 10hpf and 16hpf, on lateral (top) or dorsal (bottom) views. The black arrows indicate continued expression in the polster (pol), which changes in shape as development proceeds. tg, trigeminal ganglion.

B, *Pitx2* expression pattern at 10hpf (not expressed) and 12hpf (tg, trigeminal ganglion), on lateral views.

C, Time-course analysis of *Pitx3* expression between 10hpf and 22hpf, on lateral (top) or dorsal (bottom) views. The arrows indicate continued expression in the diencephalon (di). The arrowheads indicate an expression domain that probably corresponds to branchial arches (ba). Expression of *Pitx3* in the lens starts at 20hpf.

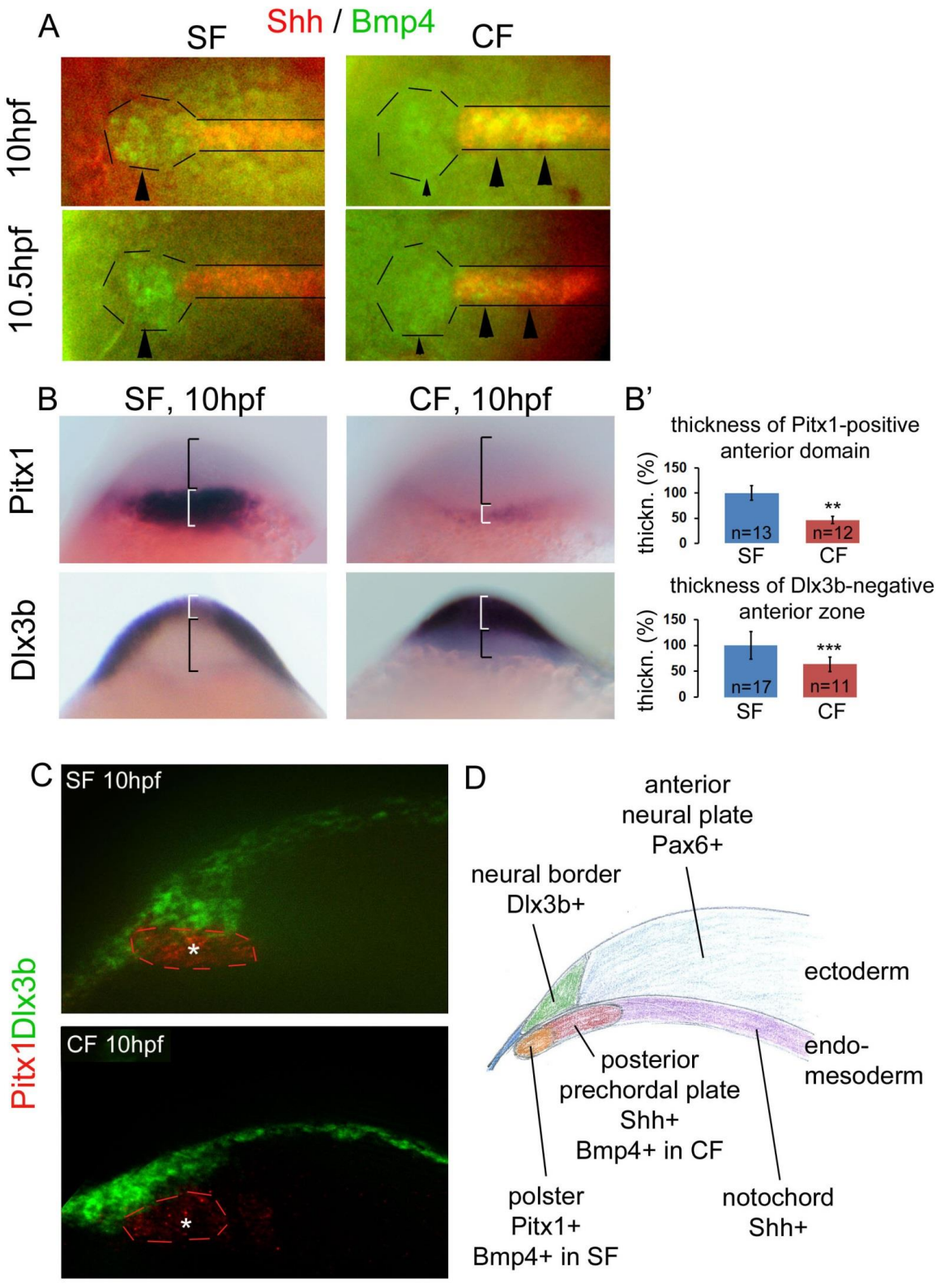

Suppl. Figure 4

Suppl. Figure 4: additional data on identification and gene expression in the prechordal plate at 10hpf.

A, Photographs of SF (left) and CF (right) embryos after double fluorescent *in situ* hybridization for *Shh* (red) and *Bmp4* (green) in dorsal views at indicated stages. The polster

and posterior pcp are delineated. *Bmp4* expression is indicated by arrows.

B, Photographs of 10hpf SF (left) and CF (right) embryos after *in situ* hybridization for *Pitx1* and *Dlx3b* (pasted from Fig. 2 for direct comparison) in frontal views. Brackets indicate regions of interest. Note that *Dlx3b* anterior expansion in CF is mirrored by an apparent thinning of *Pitx1* expression domain, and vice versa in SF.

B', Histograms showing quantification of gene expression domains in SF (blue) and CF (red) 10hpf embryos. Numbers in bars indicate the number of embryos for quantification. Data are mean±s.e.m. Significant differences are indicated: ***p<0.001, **p<0.01, Mann Whitney test.

C, Confocal views in the sagittal plane of 10hpf embryos after double fluorescence *in situ* hybridization for *Pitx1* (red) and *Dlx3b* (green). The asterisk indicates the location of the polster.

D, Scheme to help the interpretation of gene expression patterns and anatomical structures. The differences in prechordal plate *Bmp4* expression between SF and CF embryos at 10hpf are indicated.

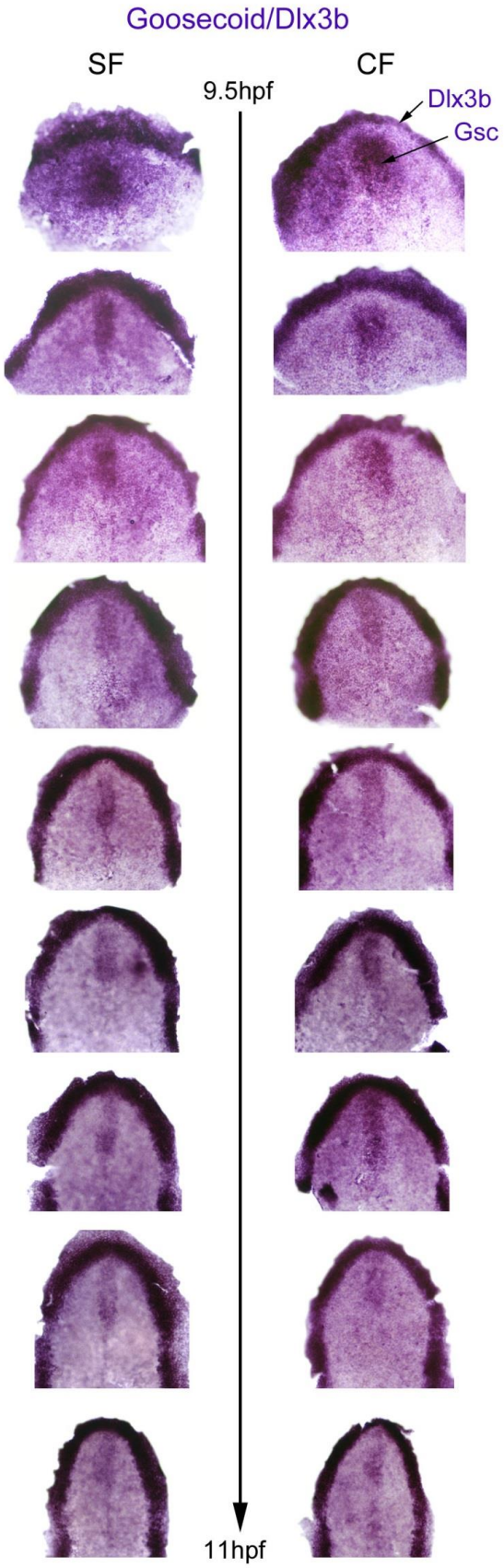

Suppl. Figure 5

Suppl. Figure 5: Comparative expression of *goosecoid* in SF and CF embryos.

Photographs of double *in situ* hybridation for *Dlx3b* (neural border) and *Goosecoid* (pcp) in SF (left) and CF (right) embryos between 9.5 and 11hpf. The two markers are in purple.

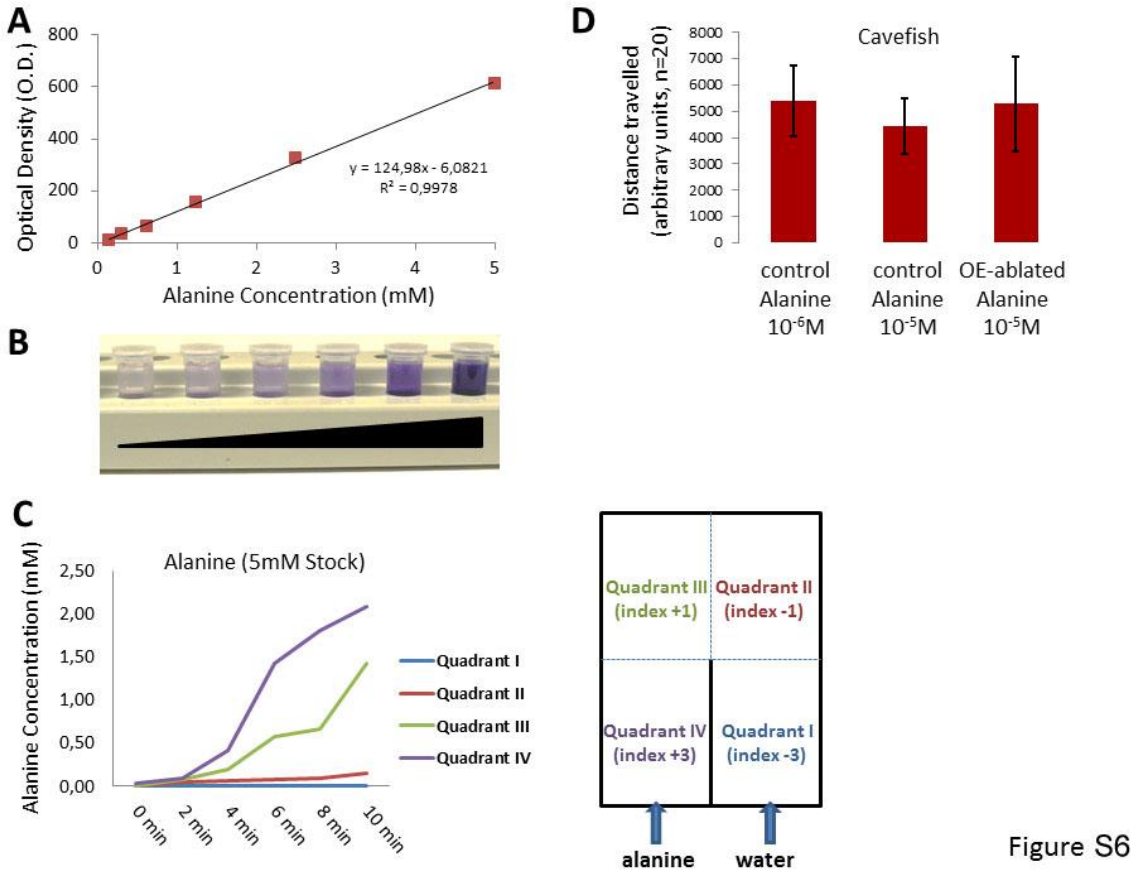

Figure S6

Suppl. Figure 6: Additional controls for olfactory behavioral tests.

A, B, Calibration curve for the measurements of Alanine concentration in the behavioral set-up.

C, Evolution of Alanine concentration in the four quadrants (noted I to VI, color-coded) of the behavioral apparatus as a function of time, after perfusion of a 5mM stock solution on one side. This curve was used to define the +3, +1, -1, -3 scores attributed to each quadrant of the box, respectively, as schematized on the left part of the figure panel.

D, Quantification of distance travelled in the behavioral apparatus during the 7 minutes of the test by CF, in various conditions.

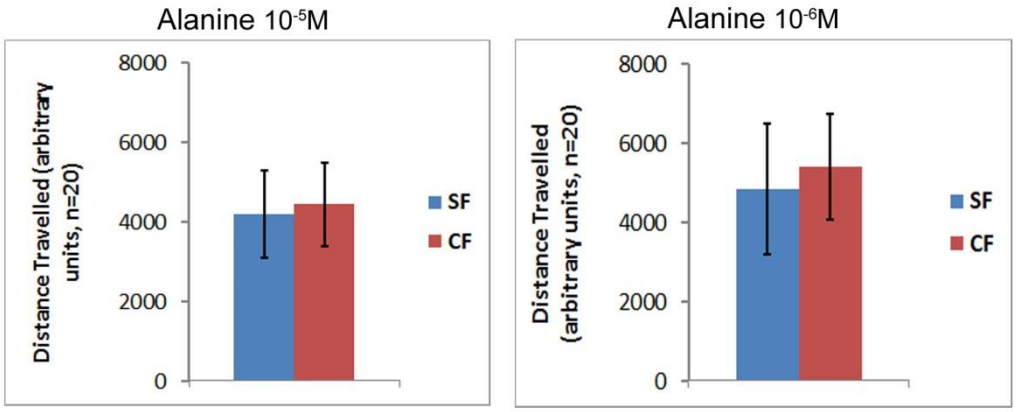

Figure S7

Suppl. Figure 7: Distance travelled in the olfactory behavioral test.

Quantification of distance travelled by CF (red) and SF (blue) in the behavioral apparatus during the 7 minutes of the test, after perfusion of Alanine 10^{-5}M or 10^{-6}M.

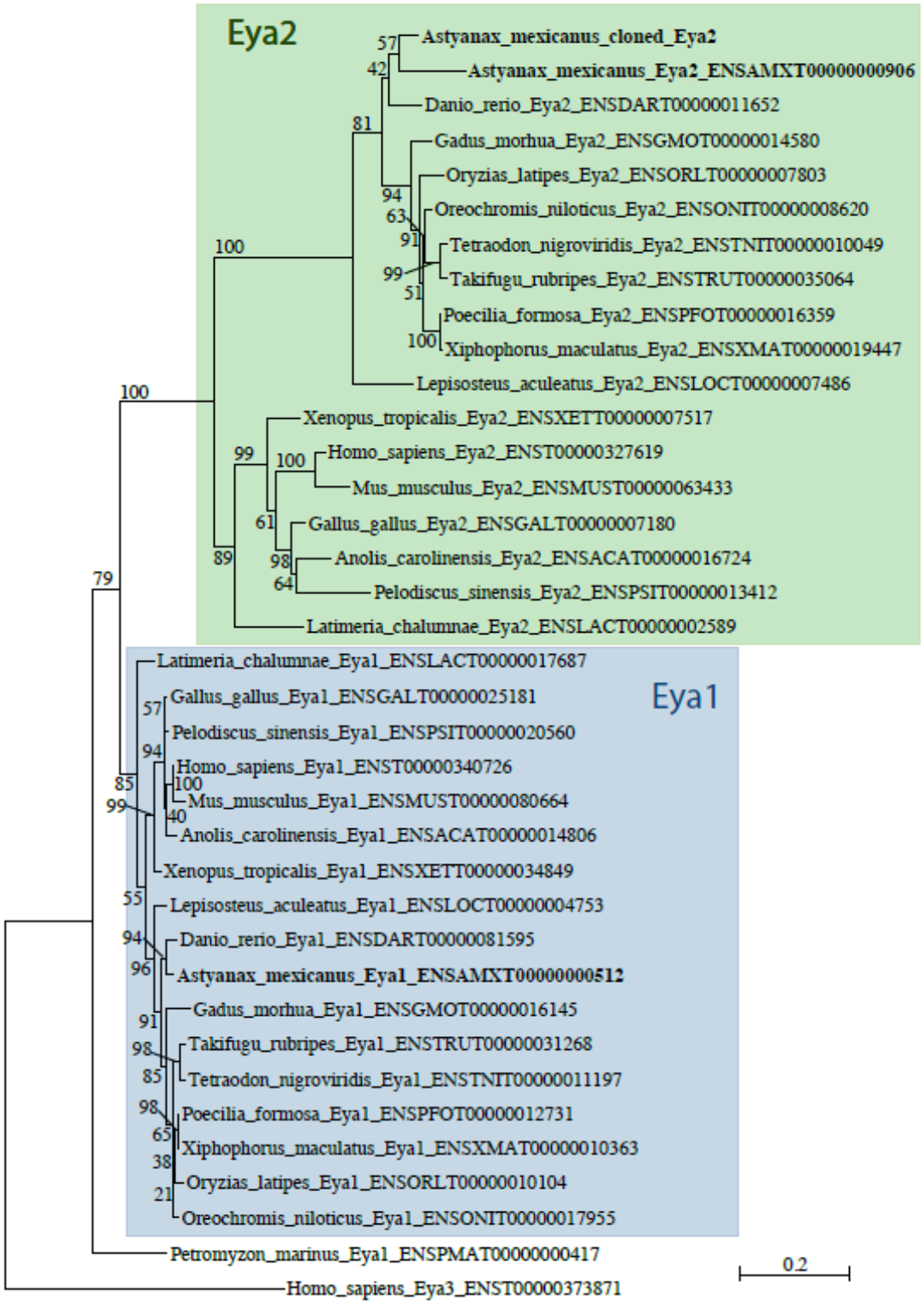

Suppl. Figure 8: phylogenetic tree for *Astyanax* Eya2. Maximum parsimony tree of vertebrate Eya1/2 protein sequences. *Astyanax* sequences (from the genome assembly and from our experiments) are in bold.

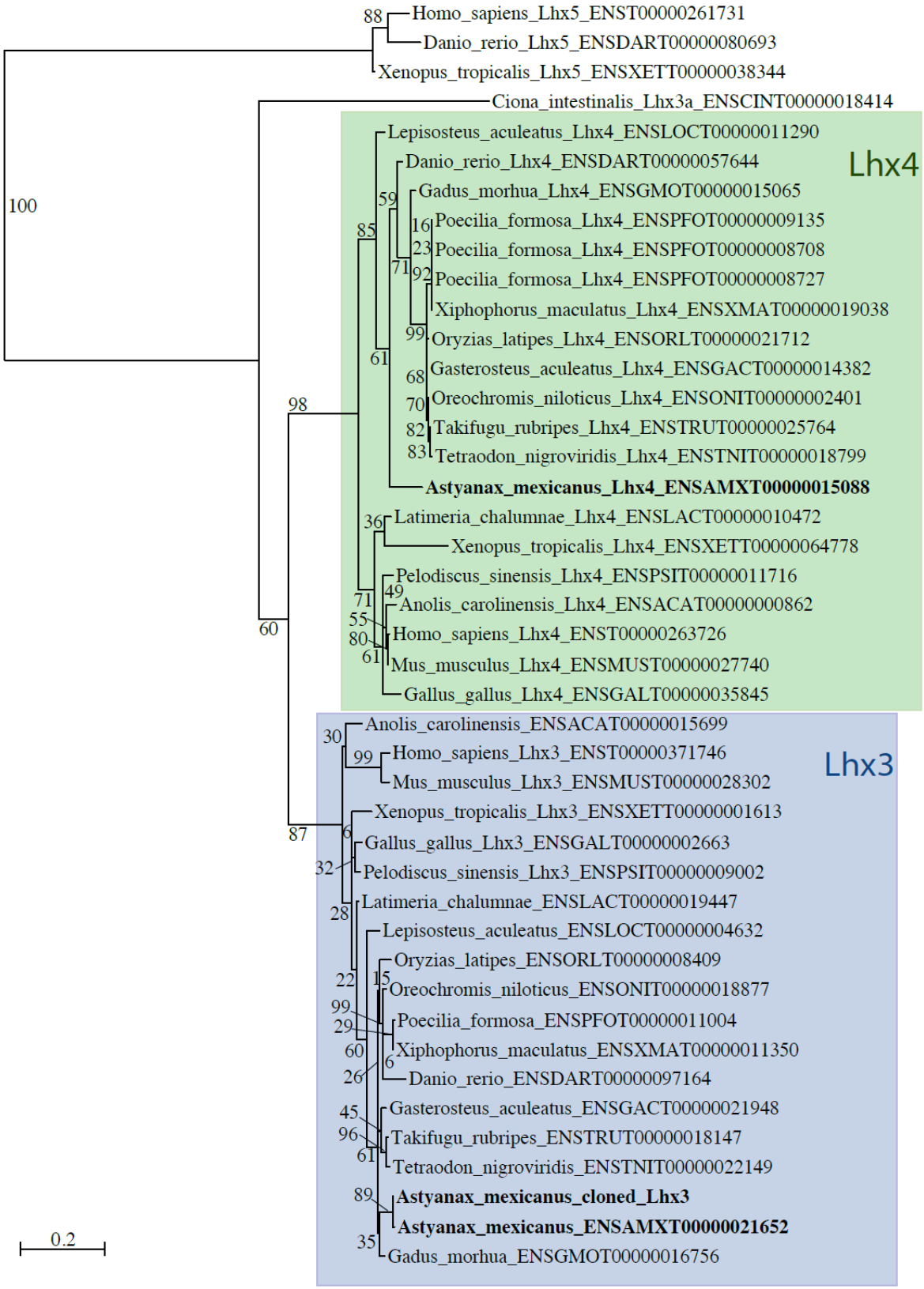

Suppl. Figure 9: phylogenetic tree for *Astyanax* Lhx3. Maximum parsimony tree of vertebrate Lhx3/4 protein sequences. *Astyanax* sequences (from the genome assembly and from our experiments) are in bold.

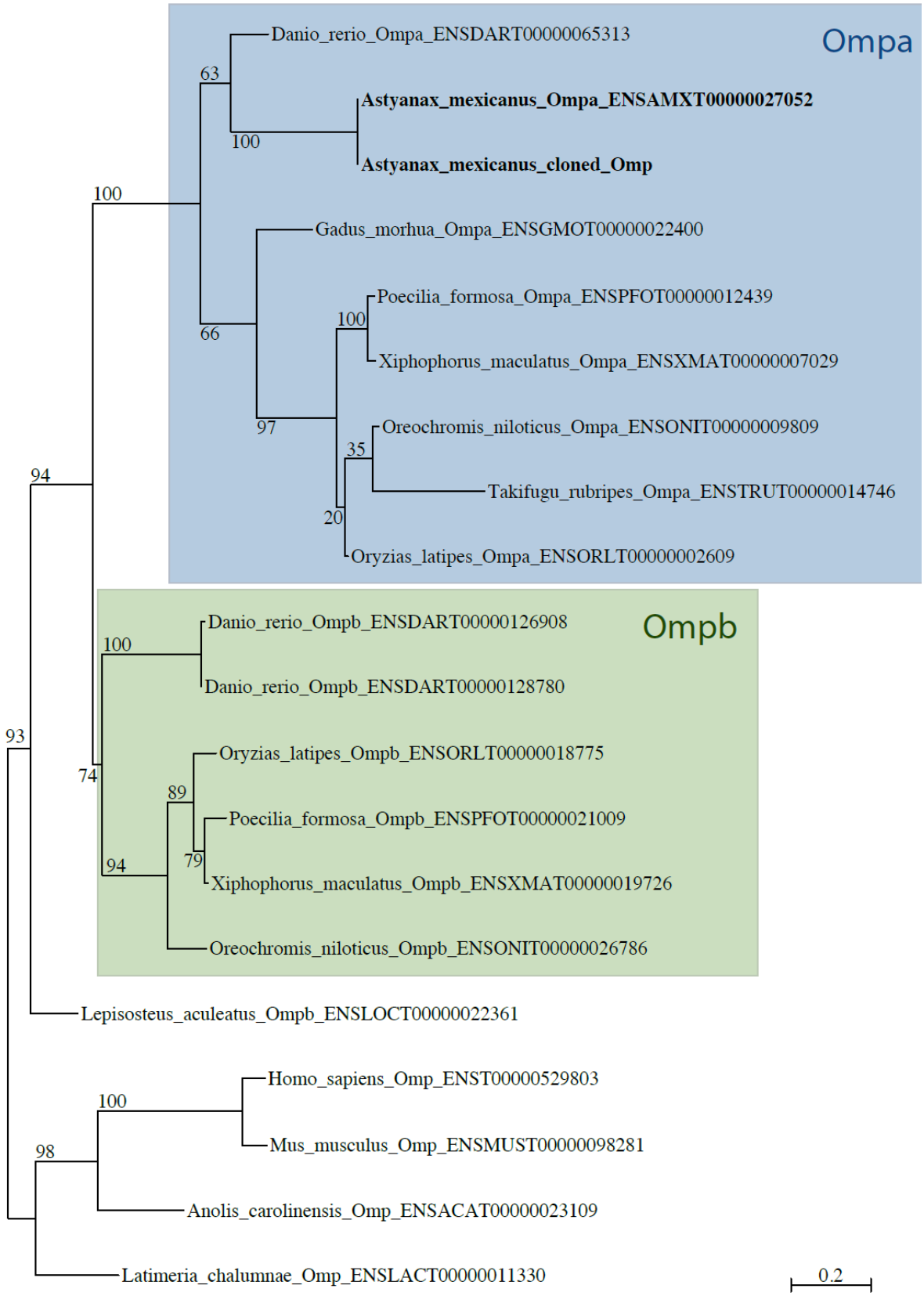

Suppl. Figure 10: phylogenetic tree for *Astyanax* OMP. Maximum parsimony tree of vertebrate OMP protein sequences. *Astyanax* sequences (from the genome assembly and from our experiments) are in bold.

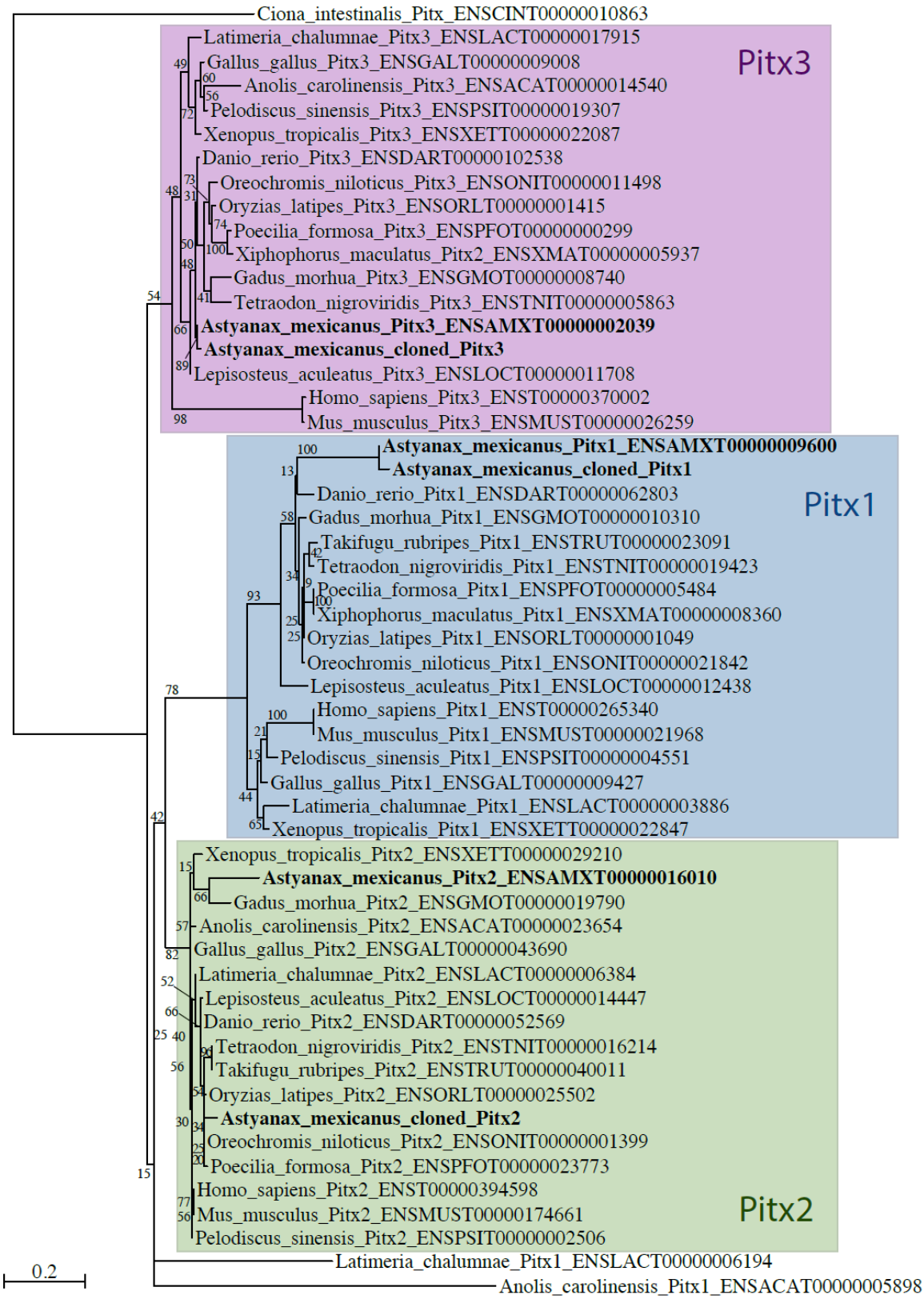

Suppl. Figure 11: phylogenetic tree for *Astyanax* Pitx1, Pitx2, Pitx3. Maximum parsimony tree of vertebrate Pitx protein sequences. *Astyanax* sequences (from the genome assembly and from our experiments) are in bold.

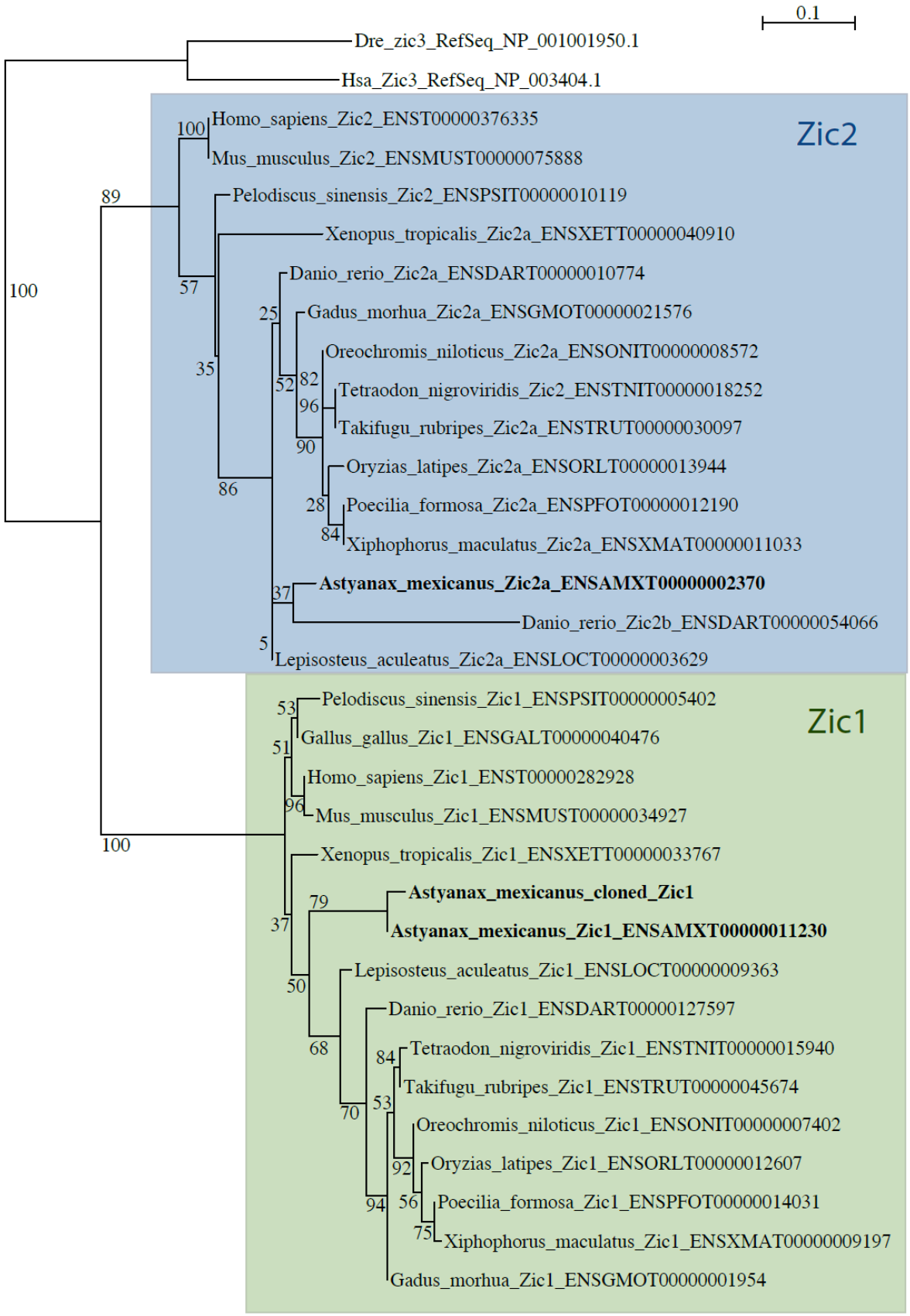

Suppl. Figure 12: phylogenetic tree for *Astyanax* Zic1. Maximum parsimony tree of vertebrate Zic1/2 protein sequences. *Astyanax* sequences (from the genome assembly and from our experiments) are in bold.

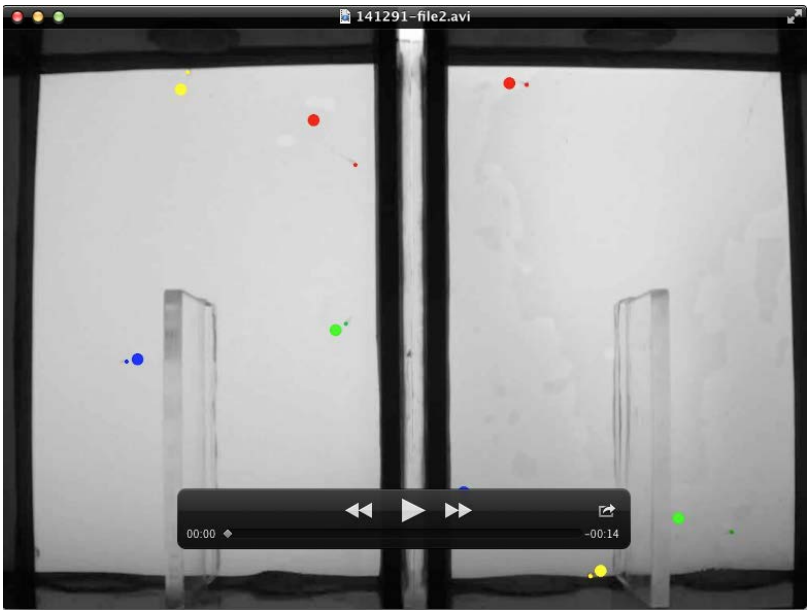

Suppl. Movie S1: Time lapse movie of a behavioral test.

An accelerated movie is shown for an Alanine 10^{-6}M test, and the four fish in each box are tracked by colored dots. The test is viewed from the top. For both boxes, Alanine was perfused at the bottom right corner, while water was perfused at the bottom left corner. The left box contains 4 Pachón CF, and the right box contains 4 SF.